Aus der Klinik und Poliklinik für Nuklearmedizin

der Universitätsmedizin der Johannes Gutenberg-Universität Mainz

Die Bestimmung von Tumorvolumina und SUV verschiedener Organe aus 68Ga-DOTATOC-PET/CTs zur Vorhersage des Überlebens von NET-Patienten nach PRRT mit 177Lu-DOTATATE

Inauguraldissertation

zur Erlangung des Doktorgrades der

Medizin

der Universitätsmedizin

der Johannes Gutenberg-Universität Mainz

Vorgelegt von

Clair Louise Wise

Aus Lübeck

Mainz, 2022

Tag der Promotion: 06. Dezember 2022

Contents

I. Abbreviations

^{18}F - Fluorine-18

^{68}Ga - Gallium-68

^{90}Y - Yttrium-90

^{99m}Tc - Technetium

^{177}Lu - Lutetium-177

AI – Artificial intelligence

CNN – Convolutional neural network

CT - Computed tomography

df – Data frame

DOTA - 1,4,7,10-tetraazacyclododecane-1,4,7,10-tetraacetic acid

DOTATOC - (DOTA^{0}-Phe^{1}-Tyr^{3})-octreotide

DOTATATE - DOTA-(Tyr^{3})-octreotate

ENETS – The European Neuroendocrine Tumor Society

ESMO – The European Society of Medical Oncology

FDG - Fluorodeoxyglucose

HU – Hounsfield units

IQR - Interquartile range

mL - Milliliter

MRI – Magnetic resonance imaging

MTV – Metabolic tumor volume

NEC – Neuroendocrine Carcinoma

NEN – Neuroendocrine neoplasm

NET – Neuroendocrine tumor

NSE – Neuron specific enolase, also known as enolase 2 (ENO2)

OS – Overall survival

PERCIST - Positron Emission Response Criteria in Solid Tumors

PET - Positron emission tomography

PET/CT - Positron emission tomography combined with computed tomography

PRRT – Peptide receptor radionuclide therapy

PSMA - Prostate-specific membrane antigen

RE – Radioembolization

RefBP – Reference blood pool VOI

RefLiv – Reference liver VOI

ROI – Region of interest

SEER - The Surveillance, Epidemiology, and End Results database

SPECT - Single-photon emission computed tomography

SSA – Somatostatin analog

SSTR – Somatostatin receptor

SSTR2A - 2A-somatostatin-receptor

SUV – Standardized uptake value

TACE - Transcatheter arterial chemoembolization

TL – Tumor load

TV – Tumor volume

VIP – Vasoactive intestinal peptide

VOI – Volume of interest

II. Table and picture directories

1 Introduction

1.1 The use of PET derived data in medicine

The therapeutic and diagnostic use of positron emission tomographies (PET) and different radiopharmaceuticals have become increasingly important in oncologic medicine. In particular for NET, nuclear medicine methods have substantially advanced the therapeutic management. PET scans combined with computer tomographies (CT) or magnetic resonance imaging (MRI) effectively detect the size and spread, as well as the functional biologic properties of tumors and are therefore an integral component of cancer staging and choice of therapy. [1]

PET scans process the radioactive radiation emitted from intravenously administered radiotracers into three-dimensional images. Examples of commonly used radiotracers for PET scans include the broadly used [^{18}F]-FDG targeting the elevated glucose turnover of cancer cells, as well as receptor-specific radiotracers, such as PSMA-ligands for prostate cancer or somatostatin-analogs (SSA) such as ^{68}Ga-DOTATOC for neuroendocrine tumors (NET).

However, even though the PET scan is a common diagnostic tool in oncologic medicine, much of the generated data is not evaluated for routine clinical application. There are increasingly more studies showing that certain imaging parameters such as the quantification of tumor mass or certain standardized uptake values (SUV) may have significant prognostic information [2-4]. The correlation between anatomical size and PET derived volume calculation has already been demonstrated for many different types of tracers and tumors, contributing to the importance of PET derived parameters or biomarkers. Thus, PET might play an important role for both anatomical segmentation and for functional visualization [5, 6]. As the assessment of this data becomes easier to implement, it is important to investigate what parameters could lead to better decisions for therapy and prognosis.

In the case of neuroendocrine tumors (NET), a high sensitivity and specificity for the detection and spread of the disease have been shown for somatostatin-analog (SSA) PET tracers (e.g. ^{68}Ga-DOTATOC) targeting overexpressed somatostatin receptors (SSTR). [7] Presently, physicians generally make prognostic assumptions with the help of biomarkers derived from invasive histological biopsies that only represent focal parts of the tumor. [8] PET/CTs however, have the advantage of being able to represent the entirety of the tumor size and its location. The patient often receives multiple scans throughout treatment to monitor disease progression and/or therapy response. [9] Additionally, due to a high tumor to background contrast, PET imaging of NETs can be used for tumor segmentation to closely approximate the actual tumor mass and reliably assign the tumor manifestation to a specific

organ system. For these reasons PET data is ideal for data analysis and worth further investigation.

Currently, few studies have specifically investigated volumetric and other digital parameters of ^{68}Ga-DOTATOC PET/CTs regarding their prognostic impact on neuroendocrine tumors. The neuroendocrine tumors are a rare type of cancer; hence datasets are not as common or as widely available as in other cancer research. Therefore, the ^{68}Ga-DOTATOC PET scans have not been studied as extensively as FDG PETs or PSMA PETs, as these datasets are more common. There have also been few studies that focus on the tumor load of specific organ systems and tumor location, which sets apart this study from other tumor quantification studies.

The semi-automatic quantification of tracer accumulation and other parameters per organ system of ^{68}Ga-DOTATOC-PET/CTs of patients suffering from neuroendocrine tumors and their correlation to overall survival (OS) and treatment response will be the subject of this study.

1.2 Neuroendocrine Neoplasms - Diagnosis and therapy

Neuroendocrine neoplasms (NEN) are a rare heterogenous group of cancer that originate from neuroendocrine cells predominantly located throughout the gastrointestinal tract. They can also originate in the lung, pancreas, adrenal glands, and other organs. [10]

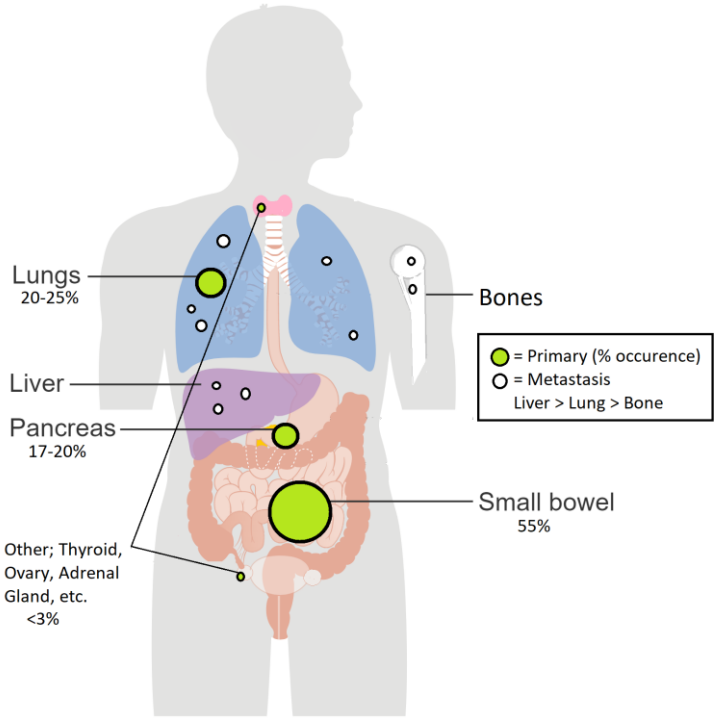

Figure 1: Distribution of primary and metastasis spread of NETs

Most cases are sporadic (85%) and generally affect patients between the ages 50 and 70, however the disease is also associated with certain genetic syndromes (15%), the most common being multiple endocrine neoplasia (MEN1). [11]
Clinically the NENs present heterogeneously, ranging from asymptomatic patients or unspecific abdominal pain to patients with functionally active NENs, that produce hormones, leading to specific secretory syndromes. One of the most secreted hormones is serotonin, in which the patient can suffer from flush, abdominal cramps and diarrhea. This syndrome is generally referred to as “carcinoid syndrome”, as the term carcinoid is a former name for NENs. Other hormones that can be secreted by functionally active NENs include insulin, glucagon, somatostatin, gastrin, vasoactive intestinal peptide (VIP), among others [11, 12].

Because of the irregular clinical presentation of these tumors, patients are often diagnosed in the later stages of their disease. The diagnosis is confirmed via a histopathologic tissue biopsy by looking for specific tumor markers, such as chromogranin A, synaptophysin and NSE. The prognosis is estimated by determining the Ki67, which is a marker for mitosis. Depending on their histology, NENs can then be classified into the following groups: the low-grade (G1-G2) well differentiated neuroendocrine tumors (NET), the high-grade NETs (G3), and the undifferentiated neuroendocrine carcinomas (NEC) [8]. So far, the only curative therapies for all NENs are purely surgical, which require removing the entirety of the tumor mass. However, as the cancer is usually diagnosed in a later stage, most therapies strive to slow disease progression and are therefore palliative. [13]

Palliative treatment options for metastatic well-differentiated NETs aim to reduce tumor burden, which can be achieved through tumor debulking, chemoembolization, receptor-targeted radiotherapy, cytotoxic drugs, inhibitors of angiogenesis or vascular endothelial growth factors, ablative methods, and liver transplantation. [14]
One of the most effective palliative strategies is targeting the SSTR2A-receptor in well-differentiated metastatic SSTR-positive NETs. The low-grade NETs generally have a high expression of 2A-somatostatin-receptors (SSTR2A), which can be measured by conducting a SSTR-PET/CT or a scintigraphy (octreoscan). NET patients in some cases, such as SSTR-negative status, may also receive a ^{18}FDG PET/CT to assess tumor-aggressiveness or for assessment of spread before operative procedures [15, 16]. ^{18}FDG PET/CT are therefore usually used for G3 NETs or G3 NECs, but in some cases are also serve prognostic purposes for G1/G2 NETs [4, 17].
If the SSTR functional imaging proves the NET SSTR-positive, a somatostatin-analog (SSA), e.g. octreotide LAR or lanreotide, may be administered as a first line therapy for low-grade intestinal NETs with small to midsize tumor load [14], according to several guidelines, e.g.

ENETS, of the ESMO (European Society of Medical Oncology) [18] and DGVS (*Deutsche Gesellschaft für Gastroenterologie, Verdauungs- und Stoffwechselkrankheiten, Empfehlungen für NETs 5.3 – 5.5*).

Key studies investigating the effect of non-radioactive somatostatin analogues with double-blind prospective randomized placebo-controlled studies have led to approval of somatostatin analogues in many NET entities. The main studies that confirmed the therapeutic advantage of SSAs are the PROMID and CLARINET study.
The PROMID study by Rinke et al. [14] showed that octreotide LAR had a significantly longer progression free survival over the placebo for metastatic midgut NETs. Similarly, the CLARINET study by Caplin et al. [19] showed that low grade metastatic enteropancreatic NETs (Ki-67 <10%) treated with lanreotide had a longer progression-free survival compared to the placebo control group.

For certain patient subgroups, e.g., exclusively hepatic spread, locally ablative procedures such as radio embolization (RE) or transcatheter arterial chemoembolization (TACE) may also be considered as a first or second-line therapy. The ablative procedures can also be used sequentially after a patient has undergone SSA or other therapies for predominantly hepatic disease progression [20].

In case of disease progression under first-line therapy, a peptide receptor radio therapy (PRRT) may be considered as a second-line therapy option for eligible patients, based on the findings of Strosberg et al. in the NETTER-1-study [21]. The NETTER-1-study found there was a significantly longer progression free survival in patients who were treated with a combined therapy of PRRT (^{177}Lu-DOTATATE) and octreotide LAR, compared to patients who only received octreotide LAR. These promising results may lead to PRRT becoming an appropriate first line therapy option for SSTR positive NETs especially in combination with SSAs.

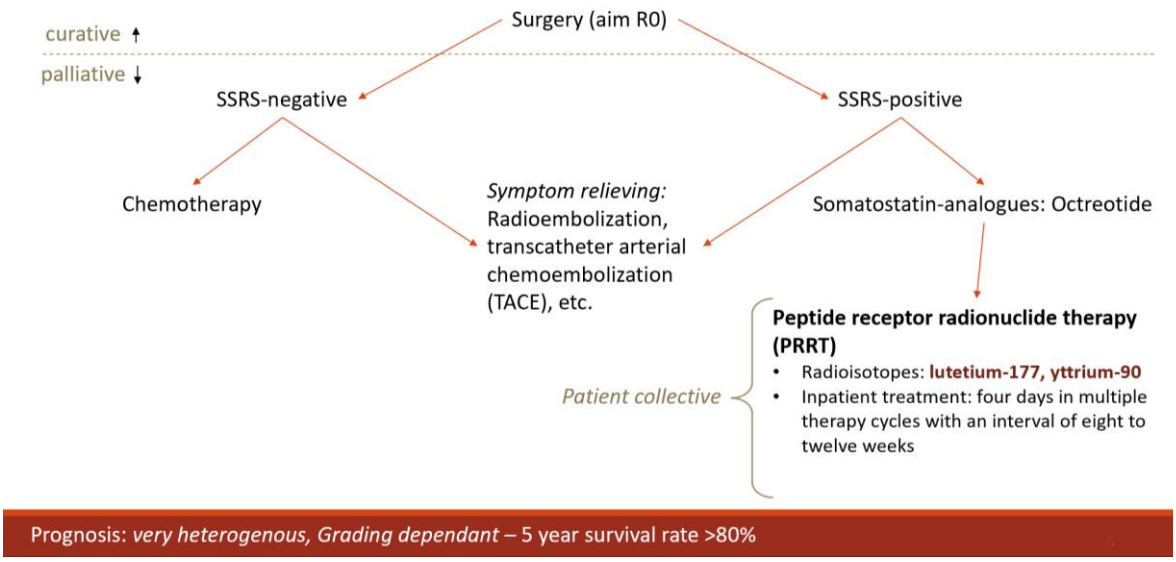

Figure 2: Simplified therapy scheme for NETs based on Pavel et al. 2016 ENETS

In order to determine PRRT-eligibility, the patient must undergo SSTR-imaging, to determine the current SSTR-status. This is known as theranostics, as both the diagnostic and therapeutic approach use the same biochemical mechanism. The tracer used for the SSTR-PET/CT is composed of a radioisotope (Gallium-68) that is conjugated to a ligand, in this case a somatostatin-analog. The most common radiotracers are ^{68}Ga-DOTATOC, ^{68}Ga-DOTATATE and ^{68}Ga-DOTANOC for NET imaging, each with different affinities for the SSTR-subgroups [22]. In the nuclear medicine department of the University Clinic of Mainz, ^{68}Ga-DOTATOC is normally used for diagnostic imaging.

For therapy, the radioligand is then paired with a therapeutic radioisotope (Lutetium-177 or Yttrium-90; both beta emitters), that can destroy the tumor mass through specifically targeted radiation. Multiple cycles of intravenous application of this chelated complex are typically applied. For this therapy the term peptide receptor radiotherapy (PRRT) has been coined. There is more data available regarding a more favorable side effect profile for Lutetium-177 compared to Yttrium-90, which is why Lutetium-177 is the more commonly used radioisotope for PRRT [21, 23]. However so far, no significant difference in overall survival (OS) has been documented between Yttrium-90 and Lutetium-177 [23], due to the lack of comparative prospective studies.

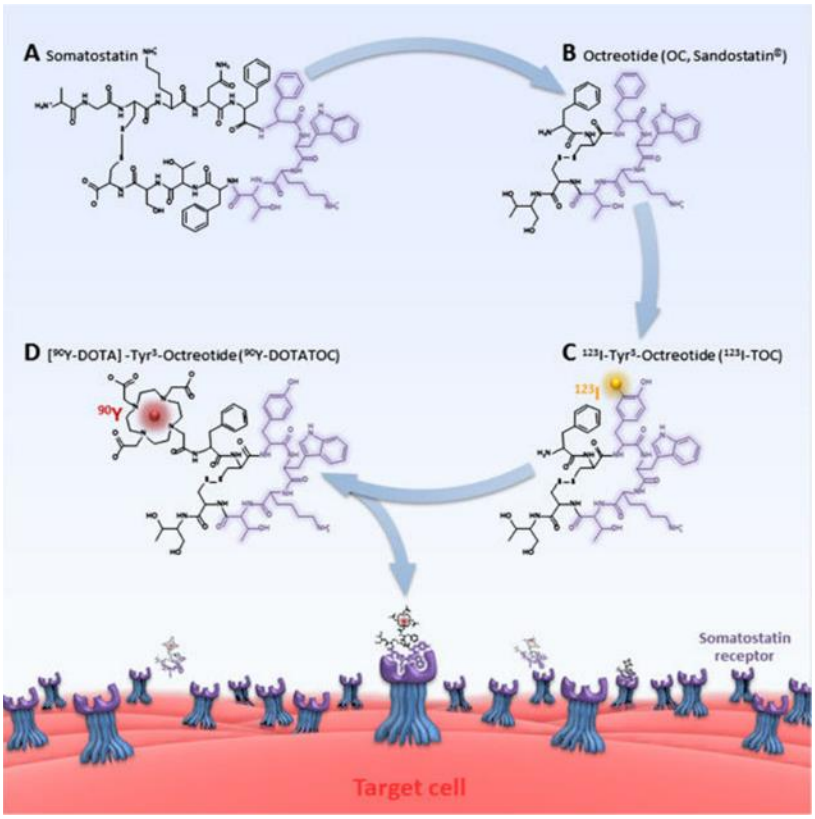

Figure 3: Formation of somatostatin analogs with the example of DOTATOC and Octreotide

Due to radioprotection regulations in Germany, peptide receptor radio therapy is an inpatient treatment that lasts three to four days in four therapy cycles with an interval of eight to twelve weeks. After PRRT, a follow-up ^{68}Ga-DOTATOC PET/CT is performed routinely to document therapy effect and receptor status – this commonly takes place around one year after the initial ^{68}Ga-DOTATOC PET/CT.

1.3 Introduction to positron emission tomography (PET)

PET scans are a useful diagnostic tool in oncologic nuclear medicine, as they differ from classical anatomical imaging (e.g., computer tomographies and magnetic resonance imaging) by showing metabolic processes and functional properties instead of tissue densities. Therefore, PETs are usually combined with a CT or an MRI to facilitate organ assignment of the radiotracer accumulations as seen in figure 4.

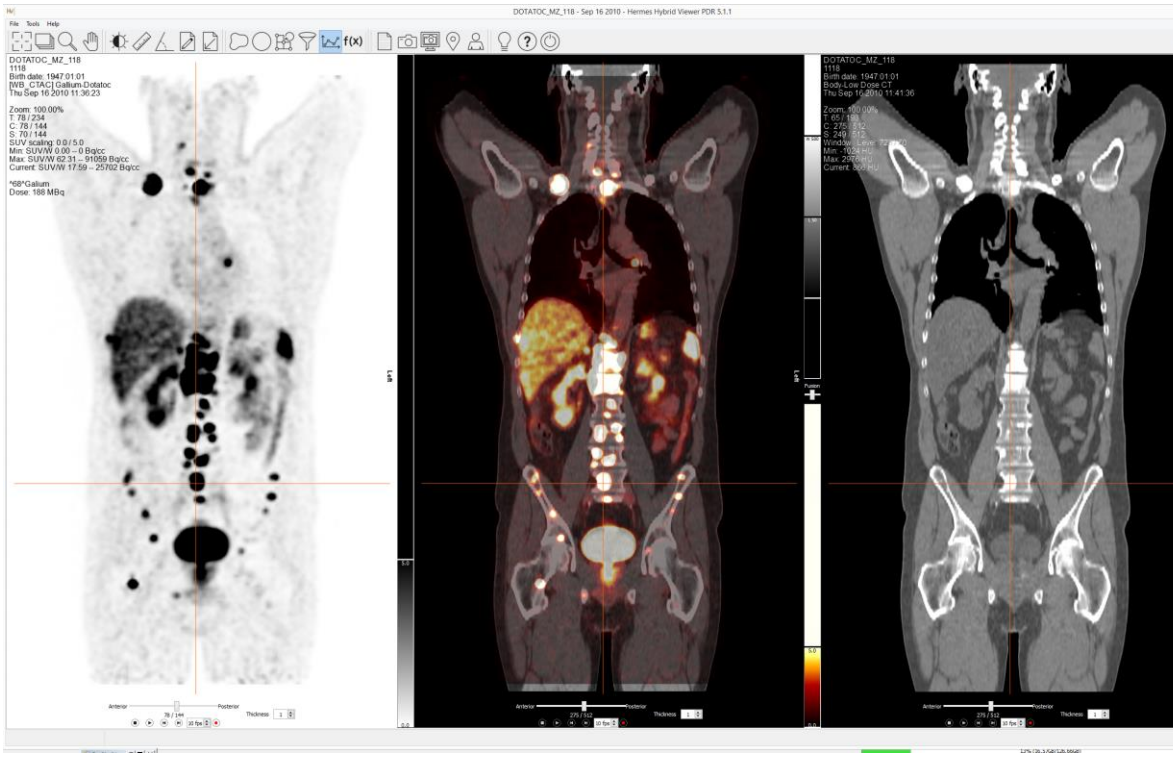

Figure 4: Example patient 118 - Combination of PET and CT to create fusion image

The radioactive tracers, also known as radiopharmaceuticals, are administered intravenously into the blood stream of the patient. The radiotracers are a combination of a ligand or drug and a beta emitting radioisotope. The ligand/drug targets a particular metabolic process, such as a specific receptor or cellular metabolism. In general, therapeutically usable radioisotopes emit beta-minus particles, whereas radioisotopes that emit beta-plus particles (positrons) are used in the diagnostic field of PET imaging. Examples of the diagnostic radioisotopes referenced in this study, include Fluorine-18 (18F) with a half-life of 110 minutes and Gallium-68 (68Ga) with a half-life of 68 minutes. These positrons only exist for a couple of nanoseconds and immediately collide with the surrounding electrons of the patient's tissue. This annihilation, in which a particle reacts with its antiparticle, causes the emission of 2 photons pointed in opposite directions (180° apart). The emitted photons will then be absorbed and processed by the PET scanner using coincidence detection.
The PET scanner consists of photon detectors arranged in a circle around the patient, allowing the simultaneous absorption of both oppositely emitted photons. This simultaneous detection of the two photons on opposite ends is computed into a so-called line of response/coincidence on which the location of the positron-electron annihilation can be estimated. This computation using the circular alignment of the detectors is known as coincidence detection and allows the creation of a three-dimensional image [24].

The following radiotracers are referenced in this study:

- ^{18}F- Fluorodeoxyglucose (^{18}F-FDG) is radioactively marked glucose and is metabolized like regular glucose. Therefore, this tracer is used to target the elevated glucose turnover of cancer cells, known as the Warburg effect. This effect describes a changed metabolism in cancer cells, in which the consumed glucose is utilized in a specialized fermentation rather than aerobic respiration [25]. As this type of energy extraction is highly inefficient, an increased glucose uptake is necessary to uphold the metabolism of the cancer cell.
  This radiotracer is the most utilized tracer in nuclear medicine as the Warburg effect is common in many types of cancer cells, meaning that much of the insight and research surrounding radiotracers is based on studies with ^{18}F-FDG.
- ^{68}Ga-Prostate-specific membrane antigen (^{68}Ga-PSMA) targets the overexpressed PSMA-receptor of prostate cancer cells.
- ^{68}Ga-1,4,7,10-tetraazacyclododecane-1,4,7,10-tetraacetic acid-Phe1-Tyr3-octreotide (^{68}Ga-DOTATOC) is one of the many somatostatin-analog-radiotracers that targets the overexpressed somatostatin-receptor (SSTR) of NETs. Other radiotracers targeting SSTR include DOTATATE and DOTANOC, with varying affinities for the different SSTR-subtypes [22, 26, 27].

Tracer uptake in tissue or tumor is specified through the standardized uptake value (SUV) - a semiquantitative parameter that is normed among PETs. The SUV is calculated through the ratio of the image-derived radioactivity concentration and the whole-body concentration of the injected radioactivity. As it is a ratio, it is a dimensionless quantity. An SUV is assigned to each voxel of the image – a voxel representing a value on a grid in the three-dimensional space of the generated image. The voxel with the highest tracer uptake is described as SUVmax, the cluster of voxels with the highest tracer uptake is known as SUVpeak. The average uptake within a defined region is known as SUVmean. These values can refer to the entire scan or within a single lesion. Figure 5 shows a PET/CT image with the tracer uptake, as well as the houndsfield units, plotted along a line drawn through the axial plane. The segmentation program can use these values to match high SUV areas with their corresponding organs.

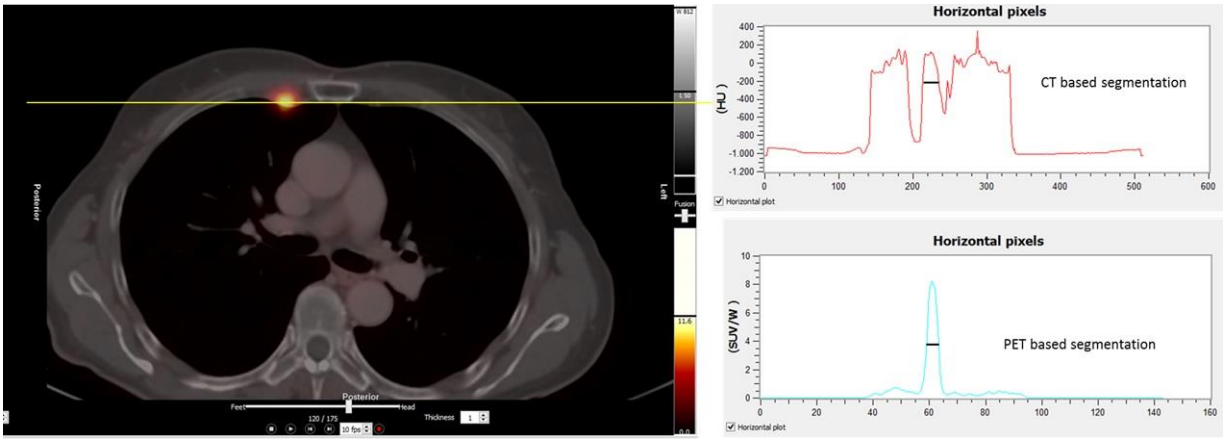

Figure 5: PET/CT image with histogram of SUV and HU along a line in the axial plane

1.4 Semi-automatic tumor quantification of PET/CTs

The extraction of imaging derived parameters from PET/CTs has become progressively easier with many automatic and semi-automatic quantification tools becoming more widely available as well as having PET/CTs become routine procedures for many diseases leading to an ever-growing database [28].

Automatic segmentation refers to the process in which an artificial neural network delineates areas in a PET/CT with high tracer accumulation and automatically assigns malignancy, organ location and generates the estimated tumor volume. The delineated three-dimensional regions are referred to as volumes of interest (VOI) (single-dimensional regions within an anatomical plane are referred to as regions of interest (ROI)). The segmentation of the VOIs can be modified by changing the parameters and threshold of the algorithm by which the program delineates.

Semi-automatic segmentation refers to the process in which this automatic segmentation is followed by manual checking and editing of the segment boundaries, as there are certain shortcomings to the purely automated process. Examples include the false labeling of organs with a physiological radiotracer accumulation as cancerous or wrong organ assignment. This usually happens when an organ with physiological tracer uptake is very close to cancerous tissue, e.g. the kidney next to a liver metastasis, causing the CCN to fuse the VOIs. In some cases, metastases also must be added, as the algorithm may not incorporate all visible tracer accumulations depending on the chosen parameters. The adding of VOIs is done by manual delineation or using automated region-growing tools, depending on what options the software has to offer. For this reason, it is important to carefully choose the parameters for the algorithm to avoid unnecessary post automated segmentation editing.

The two programs available to perform the segmentation were **PET Assisted Reporting System** (PARS) developed by Siemens Healthineers, as well as **Hybrid3D** developed by

HERMES Medical Solutions AB. Both programs were evaluated and compared for the execution of this study.

1.4.1 PARS Prototype

The PET Assisted Reporting System (PARS) by Siemens Healthineers is an application developed for the quantification of tumor mass derived from PET/CTs. Segmentation presets are available as well as customizable algorithms, that are explained in more detail in the chapter “Introduction to segmentation options of PARS”. The prototype version was intended to be used for medical research.

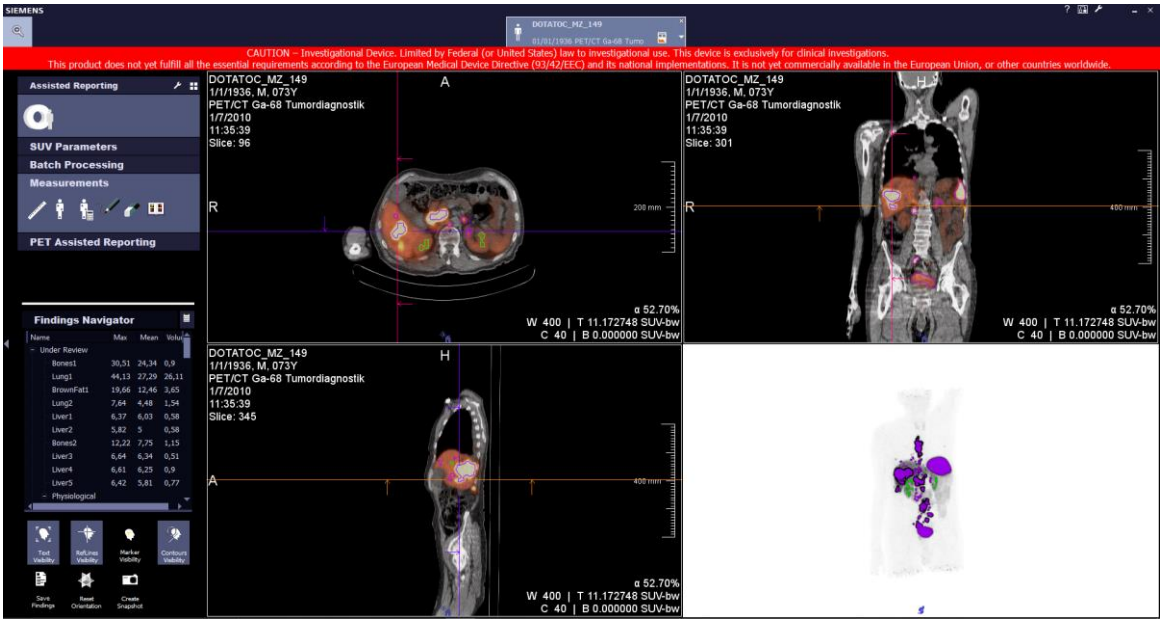

Figure 6: PARS prototype - example of 68Ga-DOTATOC PET/CT tumor quantification, transversal, frontal and sagittal plane of combined PET and CT, as well as 3D-depiction of only PET, with highlighted generated VOIs in purple and green. Left column for editing and overview of segmentation.

1.4.2 Hybrid Hermes

Hybrid3D is a clinically approved segmentation application by HERMES medical solutions AB, that provides visualization and quantification of PET and CT images. Different processing modules and presets are available for the processing of the imaging data. The use of this program is intended for medical research. (Information provided by the manual of Hybrid3D_3.0.0)

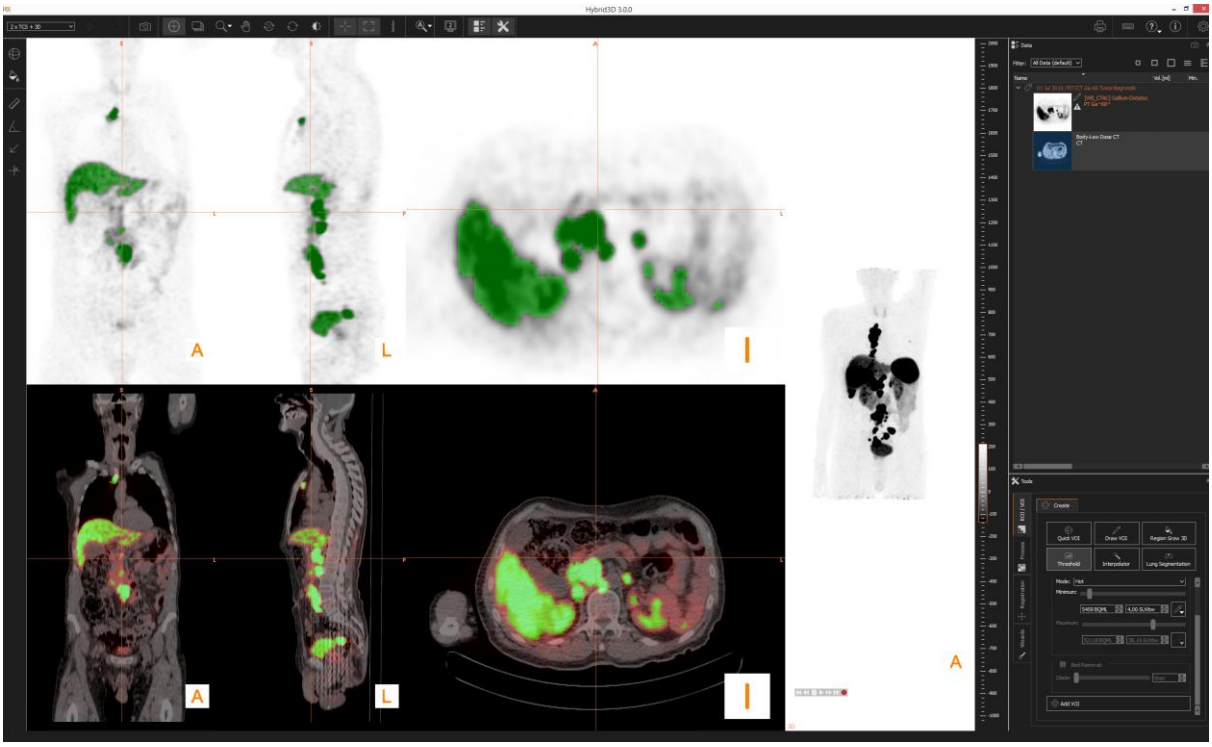

Figure 7: Hybrid3D - example patient 149, preview of segmentation at >4 SUV, editing tools and list of VOIs in the right column

1.5 The role of SUV thresholds and standardized interpretation of imaging data

For this study one of the challenges was determining parameters for the delineation algorithms that would be easily reproducible, fast, and most importantly, depict the entire metabolic tumor volume accurately. Therefore, the current segmentation methods and parameters during the time of commencement of the study were explored, to acquire a method compatible for the investigated patient collective.

The majority of the algorithms for accurate interpretation have been evaluated for the radioligand ^{18}FDG, as it is the most used ligand in nuclear medicine. This includes the influence of physiological, physical and procedural factors when interpreting SUV as a consistent parameter [29, 30], as well as the choice of segmentation algorithms and thresholding values for precise quantification of tumor volume [30]. These aspects of interpreting tracer accumulation have not been researched as extensively for other ligands,

such as ^{68}Ga-PSMA or ^{68}Ga-DOTATOC. Therefore, studies that focus on ligands other than FDG will often use procedures that were developed for FDG [2, 31], i.e. Abdulrezzak et al. who used 50% of SUVmax for both FDG and DOTATATE PET/CTs [31], as well as Ohnona et al. who used 41% of SUVmax for DOTATOC PET/CTs [2].

The main difficulty was deciding on an algorithm that would depict the NET tumor load as close to the anatomical borders as possible, as the organ assignment and volume calculation were the primary focus points of the study. In order to do this, different thresholds were determined by which the program delineates and selects the foci that are to be included in the segmentation.

According to Foster et al. finding the “true” threshold, i.e., a parameter that generates a segmentation that best represents the actual tumor boundaries, is only possible for spherical objects with a uniform uptake of the radiotracer. In clinical practice such conditions are not attainable, which is why the theoretical justification of setting a specific threshold is not always possible [30]. For this reason, most studies investigating tumor quantification will have vastly different thresholds. However, there are some types of thresholding techniques that have become more widespread than others, due to the highly accurate approximation rates with the pathological findings as well as manageability of the program [5, 6, 32].

1.5.1 Introduction to the segmentation options of PARS

The delineation algorithm of the PARS software constitutes two main components that can be altered to achieve the desired segmentation.

- **Segmentation method** - the method by which the outer boundary of the VOI is drawn to depict a lesion
  - **Inclusion method** – delineation occurs above the determined threshold, meaning that all voxels with a higher SUV than the chosen value are included in the VOI
  - **Relative method** - delineation occurs at a certain percentage (usually 40-50%) of the highest voxel (SUVmax) in automatically separated lesions.
- **Selection method** – process by which the CNN chooses foci that are to be included in the segmentation
  - **Manually set threshold** – pre-determined single value, either the highest voxel (SUVmax) or highest cluster of voxels (SUVpeak) of a VOI
  - **Adaptive threshold** - equation that uses a reference VOI placed in the liver or aorta to determine the background tracer accumulation, and adjusts the threshold based on these values

The most common approaches for segmentation are listed below:

Inclusion method with a manually set threshold - "Fixed thresholding"

Fixed thresholding describes that the threshold chosen to execute the delineation is a set value, in other words a universal value that applies to all patients.
In the case of the inclusion method, all voxels above a fixed value will be discarded and not included in the segmentation. As an example, a common value chosen is 2.5 SUV for ^{18}FDG-PET/CTs [4, 30]. This method is becoming less common, as there are shortcomings to this method, such as the overlap of foci that have a high surrounding uptake and are therefore not recognized as individual lesions.
The inclusion method can also be combined with an adaptive threshold, which is described in more detail in the following segment.

"Relative thresholding"

In the case of the relative method, delineation occurs at predetermined percentage of SUVmax, with the consensus being, that values between 40-43% of SUVmax provide reasonably accurate and reproducible results for ^{18}FDG-PET/CTs [30]. This type of segmentation has also been applied to other types of radioligands, such as ^{99m}Tc-sestamibi (MIBI)-related SPECT/CT [33], ^{68}Ga-PSMA-PET [34, 35] and ^{68}Ga-DOTATATE-PET [31, 36]/^{68}Ga-DOTATOC-PET [2]. The threshold of 42% of SUVmax was also validated by Reddy et al. [37] for ^{68}Ga-DOTATOC PET/CTs, who showed this technique had the highest correlation to CT imaging for NETs, compared to other segmentation techniques.

The pre-selection of foci for this method is either a manually set threshold, in which all foci with a smaller SUVmax than the universally set value are discarded [38], or an adaptive threshold that generates a patient-specific threshold, depending on the background tracer accumulation [3].

Adaptive thresholding describes that the threshold chosen for selection of foci is patient-specific, meaning it is individually calculated by deriving an average SUV (SUVmean) of the patient's physiological background uptake. The patient specific SUVmean can be plugged into different equations to determine an individualized threshold, so the value will be different for each patient.
The SUVmean is acquired by placing a spherical or cylindrical reference VOI in healthy liver parenchyma (RefLiv) or the aorta (RefBP *bloodpool*), typically about 1-1.5 cm in diameter.
Examples of these types of adaptive thresholding algorithms include

$$SUVthresh = 1.5 \times SUVmean + 2 \times SD$$

for ^{18}FDG PET/CTs [39], in this case the liver being the reference background VOI. Equations for other tracers, such as ^{68}Ga-PSMA PET/CTs have suggested

$$SUVthresh = \frac{4.3}{SUVmean} x(SUVmean + SD)$$

[3, 40] from a liver reference VOI as an optimal thresholding equation. During the time of the commencement of this study, there had not yet been any recommendations of adaptive thresholding for SSTR-ligand PET/CTs.

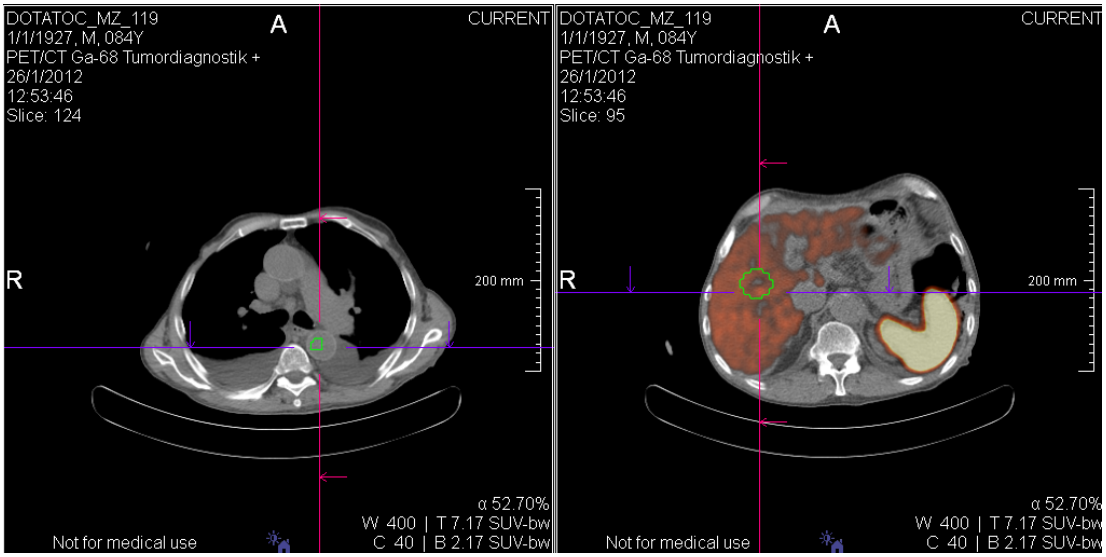

Figure 8: Example of cylindrical reference VOI in Aorta (RefBP - Bloodpool) left, and spherical liver reference VOI (Refliv) right

1.6 Convolutional neural networks in medical imaging

The automated segmentation program from PARS is based on machine learning; specifically deep learning with a convolutional neural network (CNN). This type of implementation of AI for processing radiological images has been gaining popularity in the past decade as its performance for assessing radiological images comes closer to the manual assessment. The deep learning process consists of a training and testing phase. In the training phase prepared input data (in the case of imaging data; pixels or voxels) is processed by the CNN to create output data. The CNN consists of convolutional kernels, which are small set of coefficients that determine how an output pixel is a function of an input pixel and its nearest neighboring pixels. These are applied sequentially to every pixel in an image (sometimes skipping with a stride value) to create an output image from an input image. Through combining the convolutional kernels, the CNN learns to detect complex features independently of where they appear in the image. This technology is especially useful for compensating the physiological anatomical differences between patients or finding pathologies in unexpected locations. The output data is then fed to an error function together

with teaching data. The error function can adjust parameters within the CNN to update the output data in the desired direction.

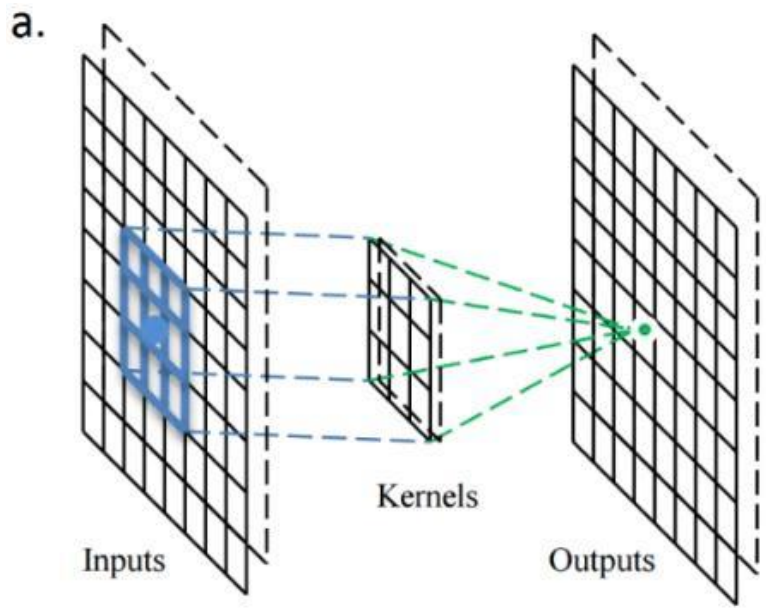

Figure 9: Input data ran through a CNN, that is made up of kernels creating different outputs

In the testing phase unseen input data is now fed to the trained CNN and once again compared to teaching data to adjust smaller errors. Unseen input data describes data that was not used in the training phase but is similar enough to test the trained CNN's capabilities. It is a proxy for the future data that the algorithm is expected to meet in the intended domain. The performance is then evaluated, and the parameters are adjusted till the CNN creates the desired output. [41]

As shown in the study by Pinochet et al., in which the PARS prototype was also used, the automatically generated metabolic tumor volumes were comparable to the manually measured tumor volumes for FDG PETs of oncological patients. However, the study does state that manual assessment of the automated segmentation is required to achieve similar results to the purely manually determined tumor volumes. [42]

1.7 Hypotheses and Aim of Study

To this day much of the data that can be acquired from PET/CTs, in particular quantification possibilities, is not used in routine clinical application. In the last decades, especially in the medical imaging field, data analysis through neural networks is becoming a big part of many new studies. This study strives to gain insight how modern image-analysis programs differ and what information can be obtained through processing the generated data.

NETs are a rare type of cancer and so SSTR-PET/CTs have not been studied as extensively as PET/CTs with other tracers, therefore a lot of insight can still be gained from investigating

these images. Similar to other studies investigating PET-derived tumor quantification, the aim of this study is to find out it if the quantification of NET tumor load derived from ^{68}Ga-DOTATOC accumulation in SSTR-PET/CTs may have a correlation with overall survival. As well as the total tumor volume, the tumor volume of specific organ systems will also be investigated, as clinically the patient will have different severity of symptoms, which may also lead to a different prognosis, depending on the spread and size of the tumor. The standardized uptake values were also documented and analyzed as the receptor density/accumulation of the tracer may also give insight into the prognosis of the patient.

These assumptions led to the following hypotheses:

1. Could the quantification of NET tumor load derived from tracer accumulation in PET/CTs have a correlation with overall survival (OS)?
    1.1. Could the quantification of tumor load of specific organ systems have a correlation with OS?
    1.2. Does the increase/decrease of tracer accumulation after PRRT have a correlation with OS?
2. Could the analysis of the SUVmean and/or SUVmax of the total tumor load have a correlation with the OS?
    2.1. Could the SUVmean and/or SUVmax of the metastases of specific organ systems have a correlation with the OS?

2 Methods

2.1 Material

2.1.1 Software

The programs that were used for the execution of this study are:

- PET Assisted Reporting System Prototype (PARS) (Siemens Healthineers) - PARS v3.0 © 2020 by Siemens Medical Solutions USA, Inc.
    - Digital imaging and segmentation of PET/CTs
- RStudio Team (2020). RStudio: Integrated Development for R. RStudio, PBC, Boston, MA
    - Survival analysis and graphs
- Microsoft Office Excel, Word, Powerpoint
    - Data sorting, graphs, image editing and documentation
- EndNote X9 © 2020 Clarivate, Boston, MA
    - Citation program
- Hybrid3D 3.0.0 © HERMES Medical Solutions AB
    - Digital imaging and segmentation during evaluation process
- HERMES Medical Solutions AB
    - Pseudonymization of patient data

2.1.2 Hardware

The following setup was used to run the PARS prototype efficiently:

- Laptop model: Alienware Area-51m
- Processor: Intel® Core™ i9-9900K CPU at 3.60 GHz
- Graphic card: NVDIA GeForce RTX 2080
- Installed RAM: 32.0 GB

2.2 Patient collective

2.2.1 Acquisition of patient data

The potential patients were collected in a protected clinic internal excel overview sheet, along with the parameters that would be important for this study, such as NET primary, number of PRRT cycles, Ki67 values, etc. These values were acquired through the internal clinic patient data base (SAP), of the University clinic of Mainz. Informed consent to obtain and analyze patient data were given within a German registry study approved by the local ethical committee.

The DICOM files of the PET/CTs were anonymized in the Hermes data base and exported to

the clinic laptop that was specifically acquired for programs that need high processing power, which allowed the PARS program to run efficiently.

2.2.2 PET image acquisition protocol

The ^{68}Ga-DOTATOC PET/CT is performed with the following settings:

- Patient
  - Pre-medication: 20 mg of Furosemide and 500 mL of Ringer's solution (deviation adapted to body weight and pre-existing morbidities), patient should also empty bladder before the procedure, Fasting is not required.
  - Patient positioning: supine position with arms over head
- Image acquisition
  - Time: 45 min to 90 min after injection of radiotracer
  - Scan length: vertex to mid-thigh (older scans start at lower orbita (skull base))
- Radiotracer
  - Type: ^{68}Ga-DOTATOC
  - Dosage: 2,0MBq/kg
- Technical equipment
  - Device: The GEMINI TF by Philips is a hybrid scanner, consisting of a multislice computed tomography (16 lines) and a positron emission tomography (time of flight PET).
  - Voltage: standard settings at 90 kV/ 60 mAs
- PET reconstruction
  - PET reconstruction protocol: Body_ctac_nac
  - Reconstruction method: BLOB-OS-TF
  - Matrix: 144 x 144
  - Slice thickness: 4 mm
- CT
  - Low Dose CT

2.2.3 Patient collective - Baseline and Follow-up PET/CT

In this study 81 ^{68}Ga-DOTATOC-PET/CTs of NET-patients with a high expression of SSTR preformed between 2009 and 2016 were analyzed. The PET/CTs chosen were performed before the patients underwent PRRT, to assess eligibility for the therapy. Out of 81 patients, 52 patients had a follow-up PET/CT approximately 1 year after undergoing PRRT (mean time between PET/CTs was 13.8 months). These images were also analyzed and included in the study to observe changes in the investigated parameters after PRRT.
The PET/CT before PRRT is referred to as the baseline PET/CT (BL), The PET/CT after PRRT is referred to as the follow-up PET/CT (FU).

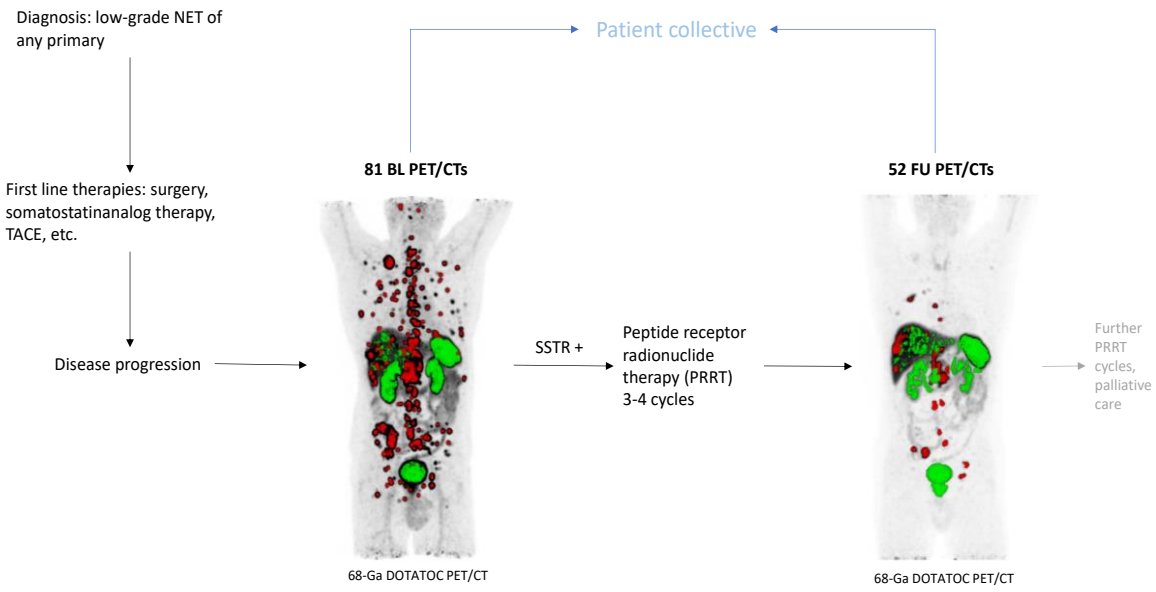

Figure 10: Patient selection dependent on SSTR status and therapy status

2.3 Quantification of tumor load using semi-automatic neural networks by PARS

The PET/CTs were processed as DICOM files, using the PARS prototype semi-automatic segmentation program. The threshold of the automatic segmentation was set to uniform parameters to ensure reproducible and fast results.

A fixed threshold was chosen for segmentation: lesions with an SUVpeak above 4 SUV were delineated at 42% of the SUVmax. SUVpeak was chosen instead of SUVmax as it avoids the exclusion of outliers [43]. Lesions smaller than 0.5mL were excluded. For evident lesions without available SUVpeak or overlapping VOIS, delineation was performed manually with the region-growing tool. This occurred 91 times out of a total of 3334 VOIs in the BL PET/CTs (2.729%) and 49 times out of 2139 VOIs in the FU PET/CTs (2.291%).

The segmentation automatically allocates the VOIs to its corresponding organ system, these can be reassigned if falsely allocated, as well as the VOI's malignancy. In this study the VOIs that were considered as cancerous were assigned to the following organ systems: bones, liver, lymph nodes, abdominal tumor load (TL), lungs and other. In some cases, the malignancy and/or the organ affiliation of the lesion was unclear (e.g., differentiating between physiological intestinal radiotracer uptake and mesenterial metastases). In these situations, an experienced specialist was consulted to assess the malignancy of the lesion. The typical organs in which there is a physiological accumulation of ^{68}Ga-DOTATOC include the liver, spleen, intestine, adrenal gland, pineal gland, kidneys, bladder and ureter.

The abdominal TL consists of mesenterial and peritoneal manifestations. VOIs lateral, and dorsal of the abdominal aorta were declared as para-aortic lymph node metastases and were assigned to the lymph node category. VOIs ventral of the abdominal aorta were considered

mesenterial metastases and therefore were assigned to the abdominal TL category. In the case in which the VOI exceeded the specified limits, the category in which the main part of the tumor mass was located was selected.

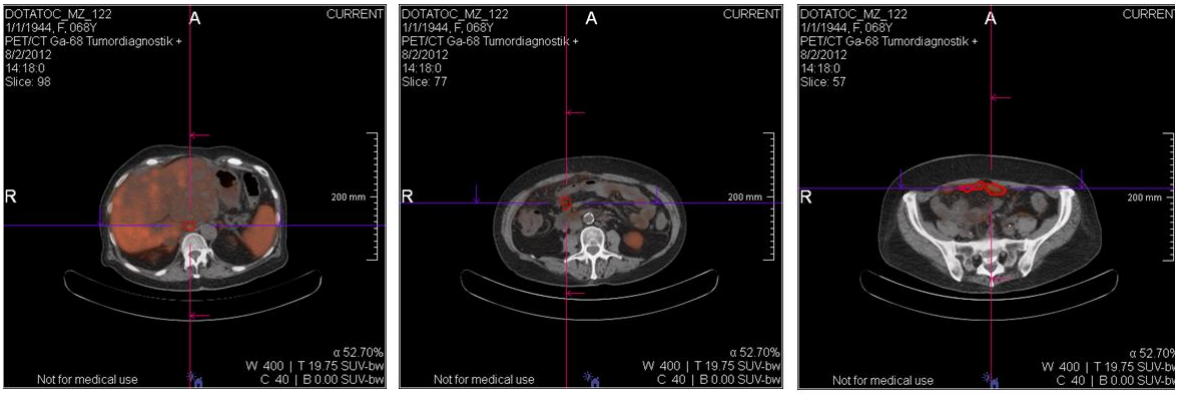

Figure 11: From left to right: paraaortic lymph node metastasis, mesenterial metastasis, peritoneal metastasis. The mesenterial and peritoneal manifestations are considered abdominal.

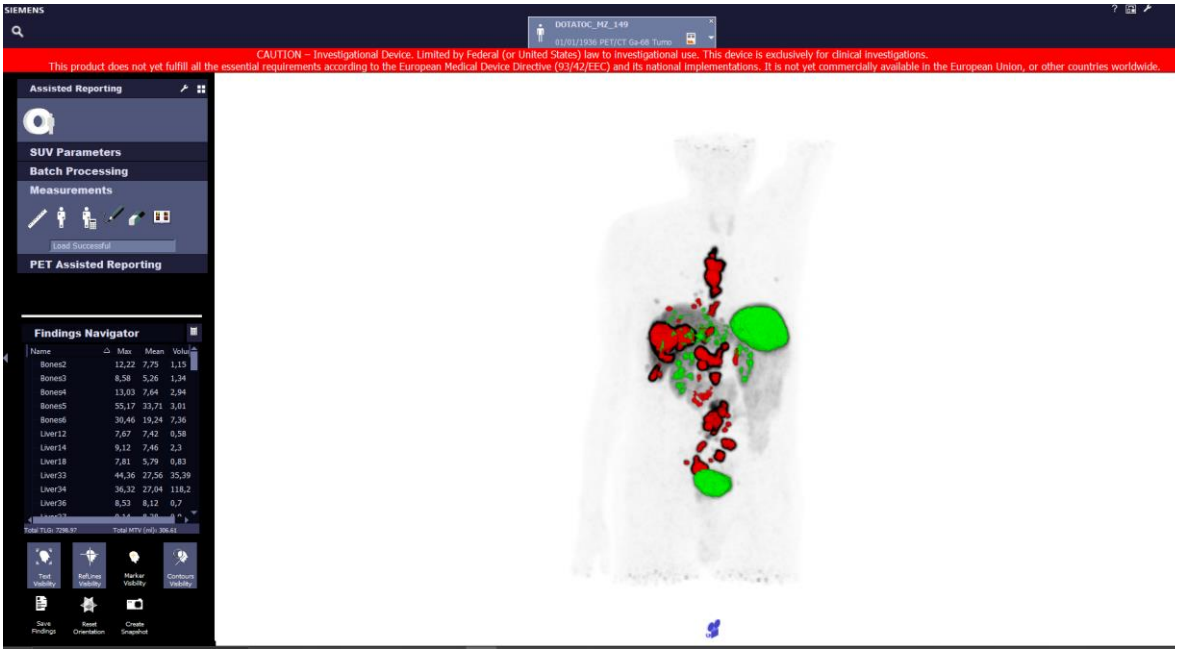

Figure 12: PARS - completed semi-automatic segmentation; red VOIs= malignant NET metastases, green VOIs = benign tissue due to physiological SSA-accumulation. The individual VOIs and their properties are listed on the left panel.

After careful examination of the generated VOIs, the data is saved as a csv data table and a transversal screenshot of each VOI is generated, as well as a screenshot of the 3D reconstruction. The csv data is processed in excel and the parameters are transferred to the main data frame in which all investigated parameters can be compared and processed using R Studio.

2.3.1 Investigated imaging parameters

Following imaging parameters were investigated:

- Volume in mL
- SUVmean (average SUV for each lesion)
- SUVmax (voxel with highest value for each lesion)

The total values as well as the values of the individual organ systems consisting of bones, liver, lymph nodes, abdominal TL and lungs were studied. Abdominal tumor load consisted of mesenterial and peritoneal manifestations. Lymph node metastases were often located in the thorax or para-aortal in the abdominal area. The lung category was combined with the category “other” due to the small sample size and was therefore not analyzed individually. The tumor volume is calculated by assessing the ^{68}Ga-DOTATOAC accumulation, therefore the SSTR expression/SSA accumulation, in other words the metabolic tumor volume, will be considered the equivalent to anatomical tumor volume for this study.

SUVmean and SUVmax were automatically generated for each lesion. The overall SUVmean of the patient was calculated in excel for total tumor mass as well as the individual organ systems. This was achieved by averaging all SUVmeans of each lesion relative to the corresponding tumor volume. SUVmax and its location were simply documented for each patient and did not require further calculations.

2.4 Specifying SUV threshold for segmentation and software evaluation

For this study both Hybrid3D and PARS were evaluated to find an appropriate method for quantifying tumor load of ^{68}Ga-DOTATOC PET/CTs. One of the main concerns was finding a threshold that delineated the tumor load as realistically as possible, while keeping the method simple and user-friendly.

Segmentation methods tested:

- Fixed thresholding with at 4, 4.5 and 5 SUV (*inclusion method*)
- Common adaptive thresholds based on other tracers (*inclusion method*)
- Custom adaptive threshold (*inclusion method*)
    - Evaluation through arterial CT images
- **Final method = 42% of SUVmax relative thresholding** with manually set threshold of 4 SUV for selection of foci

2.4.1 Hybrid3D – Fixed threshold with single value as cut-off SUV

Fixed thresholding with different cut-off values was the first segmentation method tested. With this method all voxels higher than a predetermined SUV are marked as cancerous. This is the simplest method of thresholding, but it tends to overestimate tumor mass [30]. The

values 4, 4.5 and 5 were tested, but all failed to delineate the liver correctly. This is because the mean liver background tracer uptake is often above 4 SUV (*mean SUV across 50 patients measured in Hybrid3D was 4.5*), which led to the entire liver being characterized as cancerous.

Because of this problem, it was considered to use a higher threshold for the liver and a low threshold for the remaining metastases of other organ systems. The bone, lymph node and abdominal lesions have a higher background to lesion contrast, so low thresholds are suitable for the delineation of these type of metastases. However, this type of segmentation caused double the workload and was not considered very user-friendly, which is why it was not used as the final segmentation technique.

2.4.2 Hybrid3D – Adaptive threshold pre-sets

Both the Hybrid3D and PARS program offer automated segmentation presets that have been specifically developed for ^{18}FDG-PET/CTs of oncologic patients. These presets are based on the Positron Emission Response Criteria in Solid Tumors (PERCIST). The PERCIST criteria were developed by comparing approximately 3000 FDG PETs of oncologic patients and consist of rules describing how disease progression should be evaluated based on the SUV fluctuation of the tumor mass throughout therapy [44]. The actual quantifying methods were summarized by Hyun et al. [39], on which software companies base their FDG segmentation pre-sets on.

The Hybrid3D automated tumor segmentation pre-sets are found in the tool "*Wizard Tumor Finder*" and were tested in their compatibility for ^{68}Ga-DOTATOC PET/CTs. The presets used a patient adaptive threshold equation, calculated by using a reference liver background VOI (RefLiv) to determine the mean liver uptake. The components of the equation could be manually altered, but the default parameters were set to $1.5 \times SUVmean + 2 \times SUVstdev$, which is a commonly used calculation method for the threshold of ^{18}FDG PET/CTs [39]. There were certain difficulties in implementing these segmentation methods, as there were some technical errors, as well as the VOI generation time being prolonged. In some cases, it was also difficult to place the liver reference VOI in a tumor free area, as NET patients often have multiple liver metastases. When the RefLiv VOI was misplaced in cancerous tissue, the equation would generate falsely high thresholds, causing an underestimation of the tumor mass.

2.4.3 Hybrid3D/PARS v3.0 – Custom adaptive threshold with different factors

There have been more recent studies investigating custom equations (normalized to the liver background uptake or the aorta uptake) for determining an adaptive threshold for tracers other than FDG, such as Gafita et al. for ^{68}Ga-PSMA PET/CTs [40]. As there had not yet been a validated approach for ^{68}Ga-DOTATOC, it was attempted to create an equivalent

equation for this radioligand. The validation was conducted by comparing the tumor volumes generated through different parameters, to volumes measured in the arterial phase CT. The parameter that generated the tumor volume that came closest to the CT-measured volume could then be considered as a viable segmentation option.
Following equations were considered to determine the minimal threshold:

- $SUVthresh = 1.5 \times SUVmean$
- $SUVthresh = 1.7 \times SUVmean$
- $SUVthresh = 1.9 \times SUVmean$

The tumor threshold is calculated by placing a spherical reference liver VOI (RefLiv) of about 1-1.5cm in diameter in the healthy liver parenchyma of which the mean SUV is generated. The SUVmean would then be multiplied by the factors listed above to generate a minimum patient specific threshold. These thresholds were then used to generate the volume of the tumor load as seen in figure 6.
In order to determine which factor could most accurately represent the liver tumor mass, a sample size of 10 patients with clearly definable liver metastases was compared to its corresponding arterial CT images.
The volume of the liver metastases in the arterial CT were measured manually by measuring the diameters of the transversal, -sagittal and -axial planes. The liver tumor volume generated with the different factors of the PET image was then compared to the tumor volume measured in the arterial CT. Results are listed in table 3.

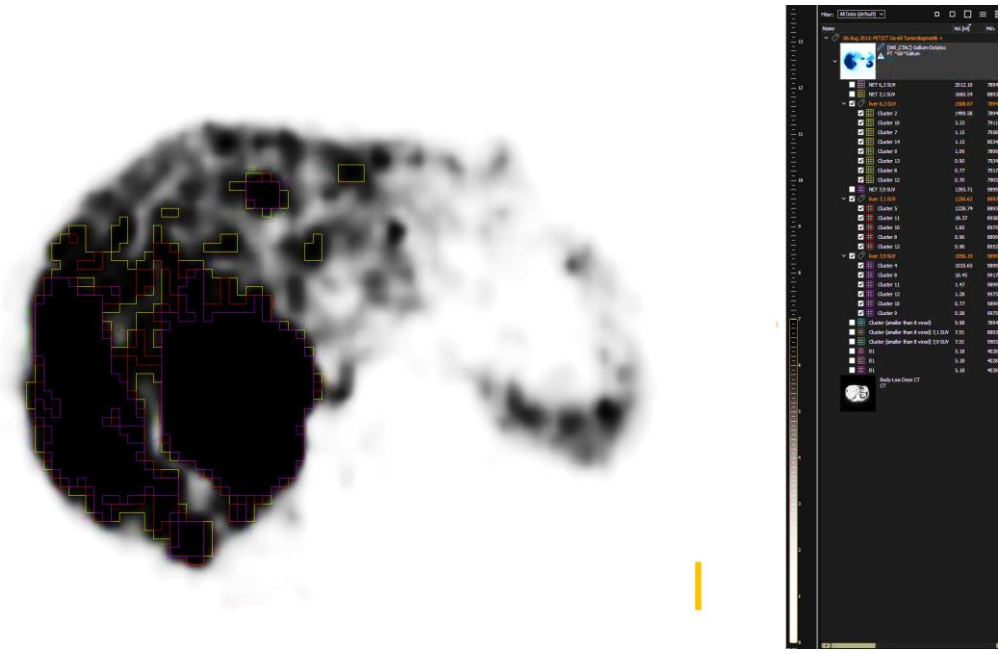

Figure 13: Custom adaptive threshold – example patient 129; Yellow = 1.5, Red = 1.7, Purple = 1.9, lesion properties are listed in the right column

Table 1: Sample size - PET patient specific threshold volume compared to arterial phase CT volume measurements

Patient ID	SUVmean of RefLiv	factor	Minimal SUVthresh	PET liver tumor volume in mL	art. CT liver tumor volume in mL	Nr liver metastases in PET	Nr bone metastases in PET	Nr abd. + LN metastases in PET
120	2.67	1.5	4	876	879.0095875	5	1	1
		1.7	4.5	770		4	1	1
		1.9	5	675		4	1	0
125	7.99	1.5	12	10		6	3	0
		1.7	13.6	3	2.78388	2	3	0
		1.9	15.2	1.5		1	2	0
127	4.82	1.5	7.2	718		3	1	1
		1.7	8.2	566		2	1	1
		1.9	9.2	455	185.04442	7	0	1
128	5.44	1.5	8.2	22		4	0	3
		1.7	9.3	14		3	0	2
		1.9	10.3	10	10.990265	3	0	0
129	4.18	1.5	6.3	1508		8	0	0
		1.7	7.1	1229		5	0	0
		1.9	7.9	1056	636.5476425	6	0	0
130	5.53	1.5	8.3	83		7	2	8
		1.7	9.4	59		6	1	7
		1.9	10.5	48	29.4287675	3	1	7
139	4.03	1.5	6.1	1029	1259.52178	8	0	0
		1.7	6.9	953		10	0	0
		1.9	7.7	892		10	0	0
141	3.16	1.5	4.7	138		18	0	6
		1.7	5.4	92		14	0	5
		1.9	6	73	50.57173	7	0	4
143	2.65	1.5	4	43		8	0	1
		1.7	4.5	31		6	0	1
		1.9	5	27	20.9778525	6	0	1
149	5.02	1.5	7.5	362	381.70088	4	2	16
		1.7	8.5	307		2	1	13
		1.9	9.5	277		2	1	14

The PET derived volumes yielded from the threshold factored by 1.9 came closest to the arterial CT volume a total of 6 out of 10 times (purple rows). Calculated from all results the best suitable factor on average to calculate a patient specific threshold is 1.79.

Issues:

- The issue of placing the liver reference VOI in a tumor free area, persisted with this technique. It was however possible to shrink the size of the reference VOI in the PARS prototype by changing the code, provided by the software architect. This made the placement of the VOI easier and the thresholding more accurate. However the placement of the RefLiv VOI still added an extra step to the segmentation process, and was therefore not as fast as a universally applicable threshold.
- The custom adaptive algorithm generally yielded very high thresholds, as seen in table 3. This led to an underestimation of boney, lymphatic, and abdominal

metastases, as these lesions tend to have a lower tracer uptake. For patients 120 and 128 the 1.9 threshold even led to the complete concealment of any abdominal or lymphatic metastases. This recurring issue highlighted that the custom adaptive threshold is not suitable for the total tumor load estimation of NETs.

2.4.4 PARS v3.0 – 42% of SUVmax relative thresholding with foci selection >4 SUV

The PARS prototype offered the relative as well as the inclusion method. The relative method conducts delineation at a percentage of SUVmax of each focus. The default setting was 42% of SUVmax, which is a proven method for FDG, PSMA and even different types of SSTR-tracers alike [30, 31, 34, 35, 37, 45]. The advantage of this method is that overlapping foci are more easily recognized as two distinct lesions, making the segmentation more exact.

Additionally, for the selection of foci, the minimum threshold was manually set at 4, meaning all foci with an SUVpeak smaller than 4 would be excluded from the segmentation. A lower threshold would not be able to accommodate the liver background activity (mean liver background activity was 4.5 SUV).
This meant that it was not necessary to set a patient-specific adaptive threshold, as the fixed threshold yielded adequate results for all patients, despite the massive fluctuation of liver background activity. The advantage of this technique is that it is also easily reproducible, as there is no liver reference VOI that needs to be positioned correctly.

This approach delineated all tumor mass adequately and rapidly, with no relevant loss of extra-hepatic metastases.

2.5 Program manageability comparison

The Hybrid3D program was the first program tested to perform entire tumor load quantification, however the PARS prototype ended up being the preferred program to conduct the study. This was mostly due to user-friendliness, program functionality, and speed.

General issues included the prolonged loading time for patients with >100 metastases as well as the user-friendliness of the programs. It was time-consuming to rename multiple metastases at once, which was important for this study, as one of the main study points is comparing organ-specific tumor mass.

The PARS prototype automatically designated malignancy to the generated VOIs and generated a very clear color-coded 3D depiction of the PET/CT. This greatly simplified the assessment of the patient's status and is one of the main advantages of PARS, as Hybrid3D did not have this function.

Both programs have difficulty delineating the liver metastases - depending on the threshold chosen for segmentation, some physiological liver activity may be included in the segmentation. The PARS prototype has the advantage of offering the relative method, in which delineation occurs at a percentage of SUVmax. This made the delineation of the liver more exact, as less overlap between foci occurred.

The transfer of volumetric data from Hybrid3D to excel was more easily manageable than the PARS program. This is because the groups - in our case organ assignment groups - that were created during segmentation, were automatically sorted in excel, making the assessment of the data incredibly efficient. In contrast the organ assignment groups in the csv files of PARS required manual reorganization for a clear overview of the excel sheet.

Hybrid3D offered the option of creating custom groups with optional color-coding for the organization of the generated VOIs - this made the visualization and comparison of different thresholding options easier. This function was not available in the PARS prototype.

2.6 Statistical Methods

The analysis of the investigated data was conducted with RStudio an open-source program which uses R - a programming language for statistics and graphics. The libraries used for the survival analysis and creation of Kaplan Meier graphs were “survival, survminer, readxl, tidyr and dplyr”, which are part of the survival package by Therneau [46].

81 PET/CTs and 52 follow-up PET/CTs performed during the time frame of 2009 to 2016 were the object of investigation, the observation period and inclusion in the data set extended till 2021. There were three imaging parameters investigated; volume of tumor mass, SUVmax and SUVmean for the entire patient, as well as the four investigated organ sets (abdominal, bone, lymph node and liver tumor mass). Non-imaging parameters were also investigated and included clinical, histological, and biological factors. All investigated parameters are shown in descriptive tables in the results section.

The endpoint of the study is considered cause specific NET-related death. The patients with no event or non-NET-related death were right-censored (non-NET related death occurred twice). Significance of the study was measured in 95% confidence intervals with a significant result having a p-value of ≤0.05. The parameters were analyzed via univariate and multiple cox regression with the end point being overall survival (OS) measured as of the BL PET/CT or the FU PET/CT respectively. These survival models are based on the standards by Therneau et al. [47]. A hazard ratio (HR) of 1 implies that there is no measurable effect on OS, a HR <1 signifies a positive effect on OS, whereas a HR of >1 indicates a negative effect on OS.

The relative tumor mass increase/reduction value was calculated by using linear regression on their logarithmic values. This was used to demonstrate accurate relative volume fluctuation.

The visual representation was performed via scatter charts, pie charts, box plots to show the dimensions and distribution of the investigated parameters. The Kaplan-Meier survival curves were generated for different patient subgroups, either divided by the median of the respective category or between different subgroups.

2.7 Follow up information acquisition

Follow up data was acquired by gathering information from the internal clinic data base SAP to document the patient's clinical symptoms and survival status. The cancer registry of the Rhineland Palatinate was also consulted in the case of patients that were lost to follow up.

3 Results

The data was processed using RStudio and Microsoft Excel via univariate cox regression and multiple cox regression. The overall survival (OS) was the main focus of the patient collective with the main event being NET-related death. The OS was measured in survival months as of BL PET/CT or FU PET/CT respectively.

3.1 Data overview

3.1.1 Descriptive patient data

Table 2: Descriptive patient data

Descriptive data	n
Age	
Median, interquartile range (IQR)	68 (59.75–75.25)
Range	22 - 85
Sex	
Male	47
Female	34
Primary tumor site	
Duodenum	34
Pancreas	24
Lung	6
Other (stomach, rectum, thymus, mamma, kidney, liver)	17
Spread of metastases	
only 1 organ system affected	6
2 organ systems affected	32
3 organ systems affected	26
4 organ systems affected	17
Functionality	
Active	23
Non-active	42
Unclear	16
PRRT	
Lu-117	81 (cycles on average 3.36)
Y-90 and Lu-117	7
Survival status	
Deceased	48 (2 excluded due to none-NET-related death)
Average survival months as of BL PET/CT	50.7 months (44.4 months exclusively deceased)
Median survival months as of BL PET/CT	47.5 months (38.7 months exclusively deceased)
Average time between BL and FU PET/CT	13.8 months

In total the study encompassed 34 women (42%) and 47 men (58%). The median age is 68 (range: 22–85, IQR: 59.75–75.25). The NET primary most commonly originated in the duodenum, a total of 34 times, in the pancreas 25 times and in the lungs 6 times. 17 patients had other primary tumor sites, including stomach, rectum, thymus, breast, kidneys, and the liver. 23 Patients had functionally active NETs and 42 were non-active. For 16 patients it was not possible to identify if the tumor was hormonally active, due to pre-existing diseases such as colitis, state after gastrectomy or other bowel-removal procedures, these patients were coded as “unclear”. All patients underwent multiple PRRT cycles of Lu-177 (on average 3.36 cycles), of which 7 patients additionally had multiple cycles of Y-90.

Of the 81 patients 46 are deceased, of which 2 patients were censored due to none-NET-related deaths. The average survival time was 50.7 months measured as of the BL PET/CT. On average the time passed between the BL PET/CT and the FU PET/CT were 13.8 months.

The non-imaging parameters investigated included: sex, hormonal activity/functionality of the tumor, origin of the tumor (NET primary location), the main manifestation of the tumor and the ki67 values. These values were acquired through the internal clinic patient data base of the University of Mainz.

3.1.2 Tumor volume and organ-specific tumor burden increase/decrease

Table 3: Overview of tumor load

Subgroups:	n of BL (mean tumor volume)	n of FU (mean tumor volume)	n of FU (Mean tumor volume difference)	Mean percentage vol difference
Entire TL	81 (317.48 mL)	52 (290.4 mL)	52 (48.26 mL)	Decrease 15.2%
Bones	40 (67.61 mL)	23 (62.84 mL)	23 (-0.31 mL)	Increase 0.5%
Liver	73 (278.62 mL)	47 (250.59 mL)	47 (44.09 mL)	Decrease 15.8%
Lymph nodes	41 (18.72 mL)	27 (13.79 mL)	27 (4.33 mL)	Decrease 23.1%
Abdominal TL	62 (28.71 mL)	40 (22.05 mL)	40 (6.72 mL)	Decrease 23.4%
Other	7 (1.52 mL)	3 (1.16 mL)	3 (/)	/

The mean tumor volume was 317.48 mL, which largely consists of liver tumor mass, as it is one of the main routes for metastases for midgut NET tumors, which constitutes the majority of the patient collective.
All tumor sites usually experienced a volume reduction after PRRT except for the bone tumor mass, which had an average increase of 0.31 mL.

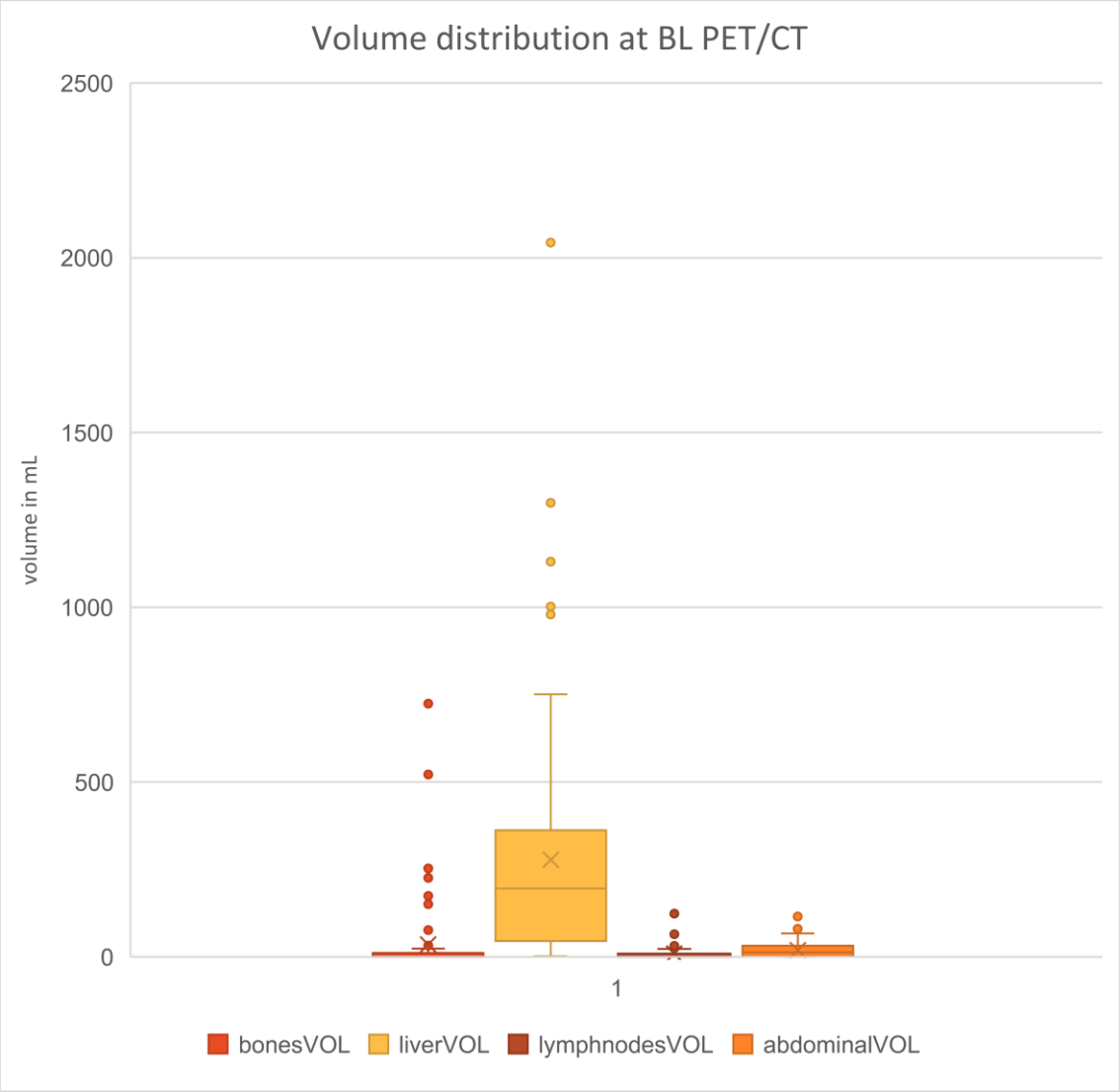

Figure 14: Volume distribution at BL PET/CT of the organ specific segmentation in PARS

The main bulk of the tumor mass, recorded at the BL PET/CT, was hepatic, averaging at 278.62 mL. Bone tumor load averaged at 67.61 mL, lymph node tumor load at 18.72 mL, and abdominal tumor load at 28.71 mL. This shows a great difference in magnitude between hepatic and non-hepatic tumor load.

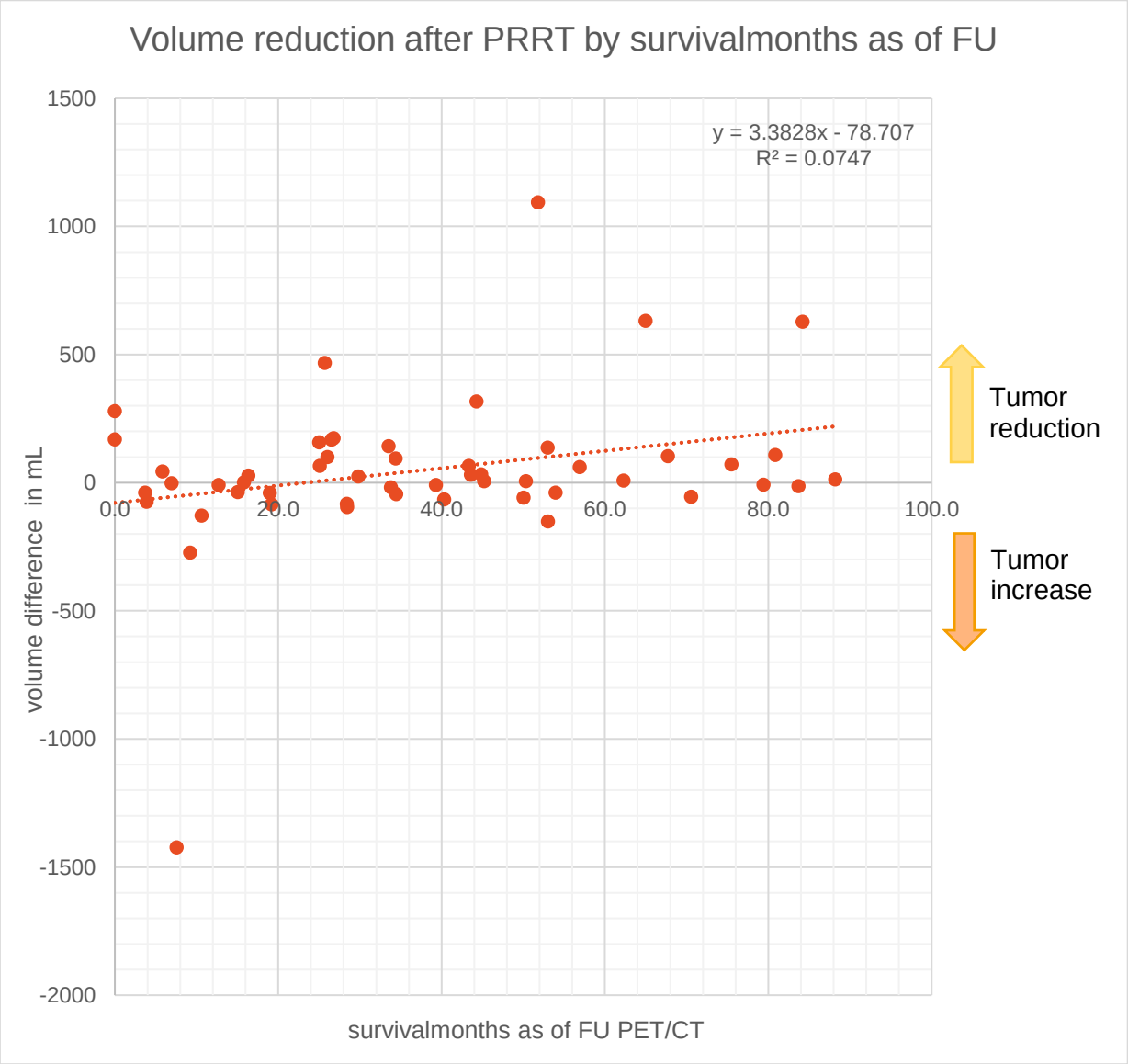

Figure 15: Overview of tumor volume reduction by survival months as of FU PET/CT

Most tumor volume reduction/increase was less than 500 mL. There were, however, some remarkable outliers with extreme tumor volume reduction/increase of over 1000 mL. The highest tumor reduction/increase was predominantly liver tumor mass, as seen in the image examples of the biggest volume differences in fig. 17-19.

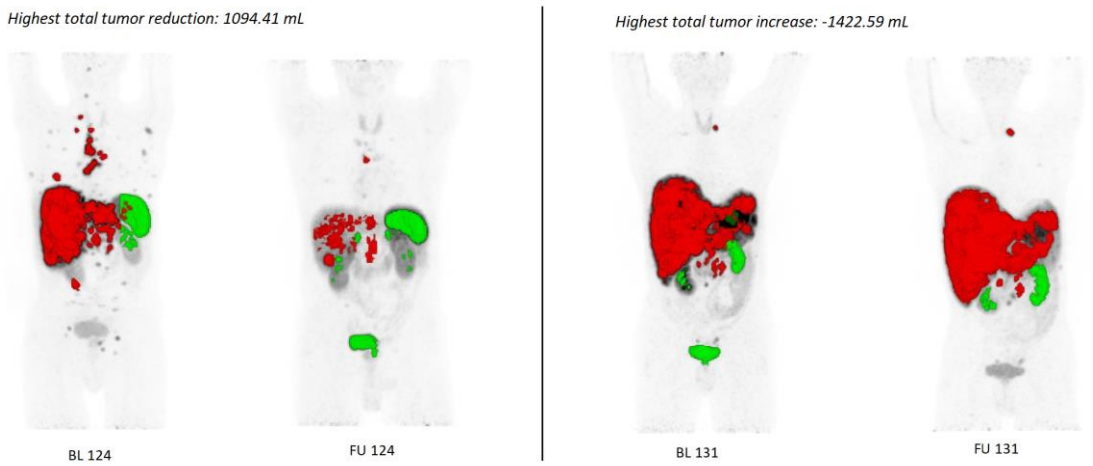

Figure 16: Visual representation of highest total tumor volume reduction and increase, primarily located in the liver

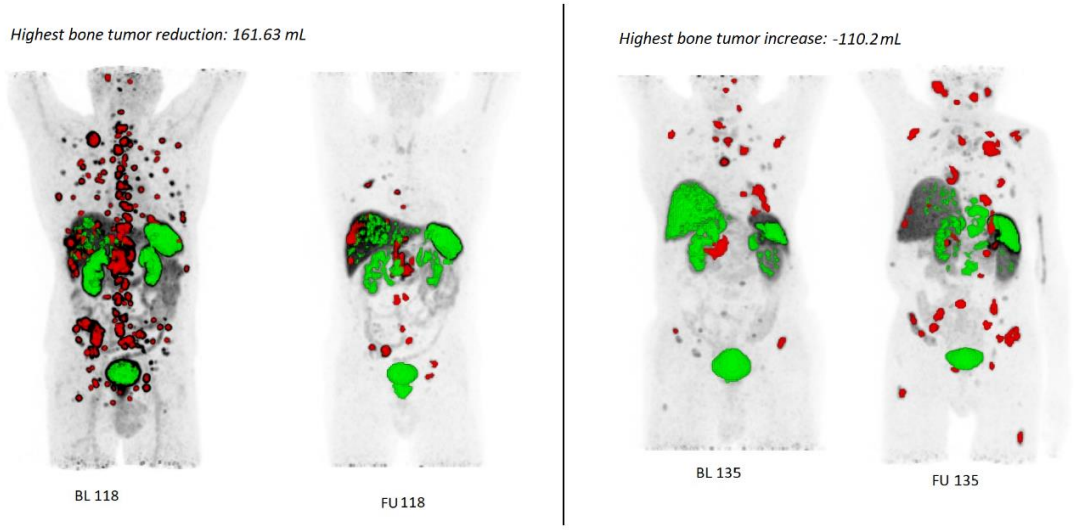

Figure 17: Visual representation of highest bone tumor volume reduction and increase

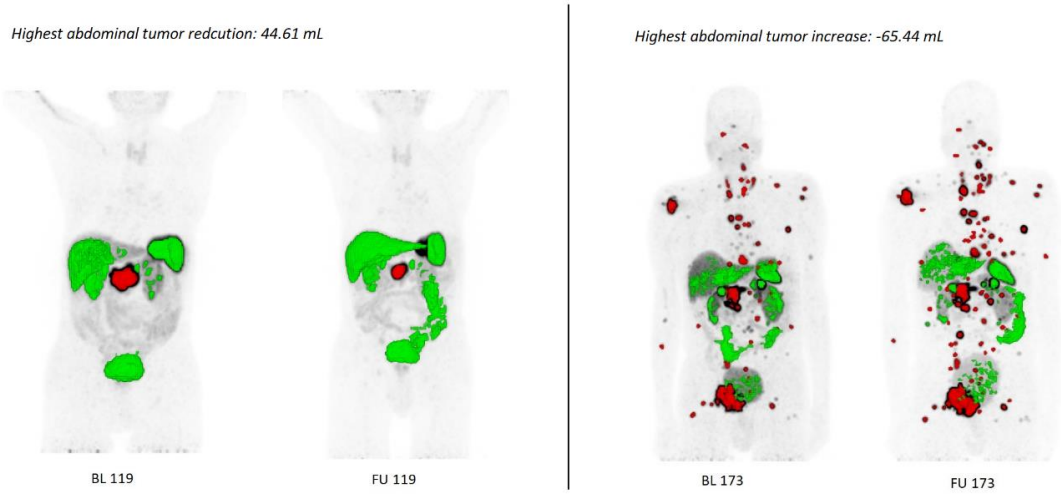

Figure 18: Visual representation of highest abdominal tumor volume reduction and increase

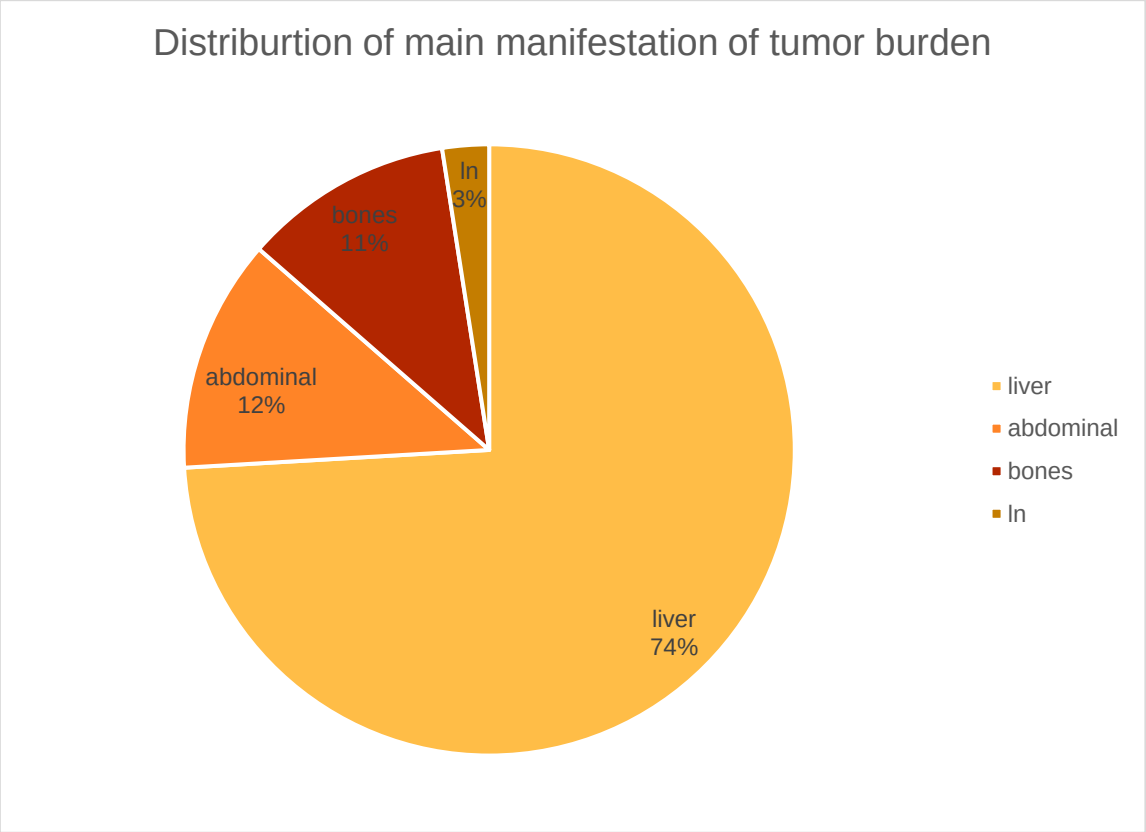

Figure 19: Distribution of the main manifestation of tumor mass in the patient collective

The pie chart shows that the majority of patients presented with a main tumor manifestation in the liver. Less than 26% of the patient collective presented a main tumor manifestation in non-hepatic tissue.

3.1.3 Scatter charts of investigated parameters: Volume, SUVmean and SUVmax

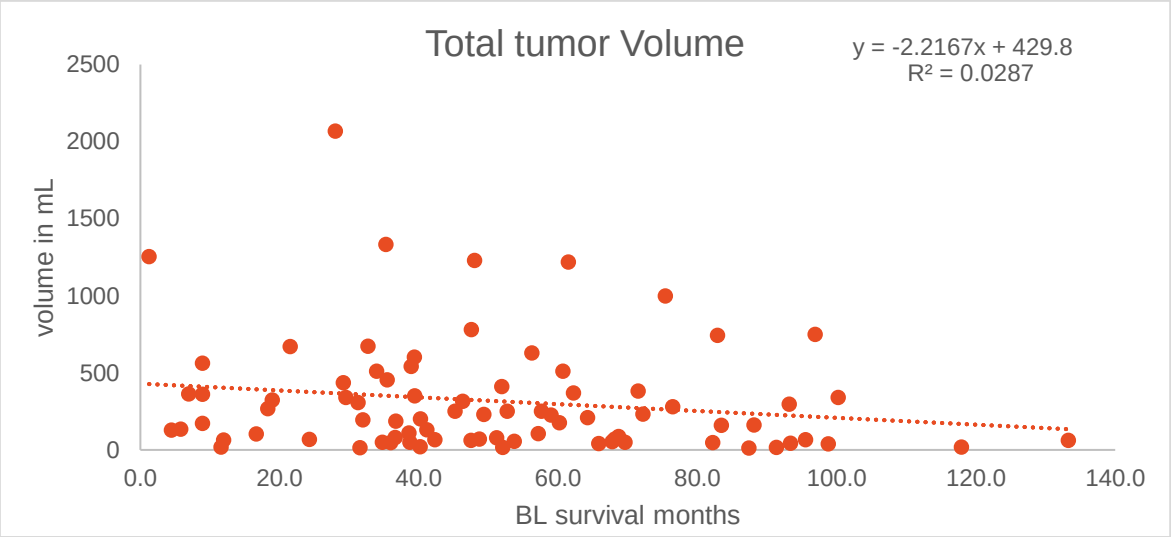

Figure 20: Total tumor volume to BL survival months distribution

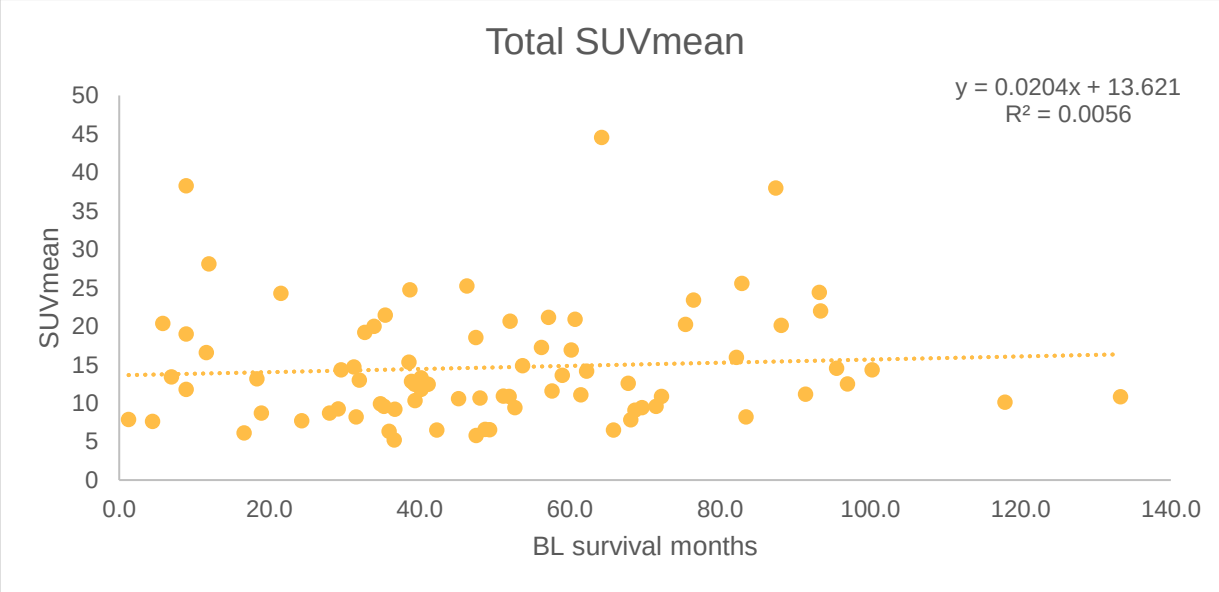

Figure 21: Total tumor SUVmean to BL survival months distribution

Low total tumor volume and prolonged survival months do not show a strong correlation however the trendline does show a negative slope, which may point to an anti-proportional correlation. The trendline of total SUVmean and BL survival months do not show any correlation. The R^2-values for both graphs are low indicating that the distribution does not correlate strongly with the trendline.

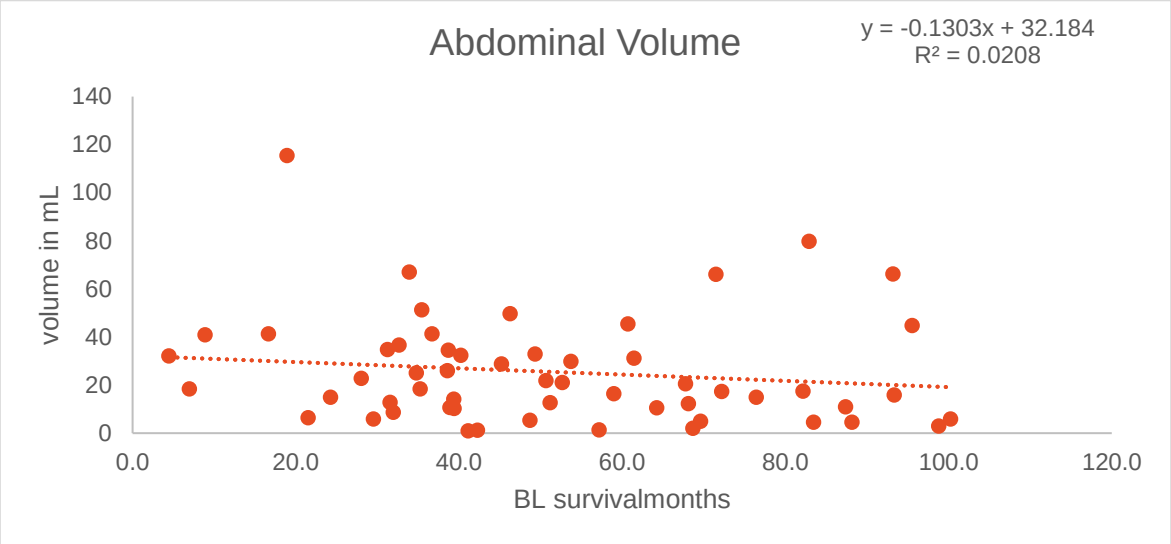

Figure 22: Abdominal Volume to BL survival months distribution

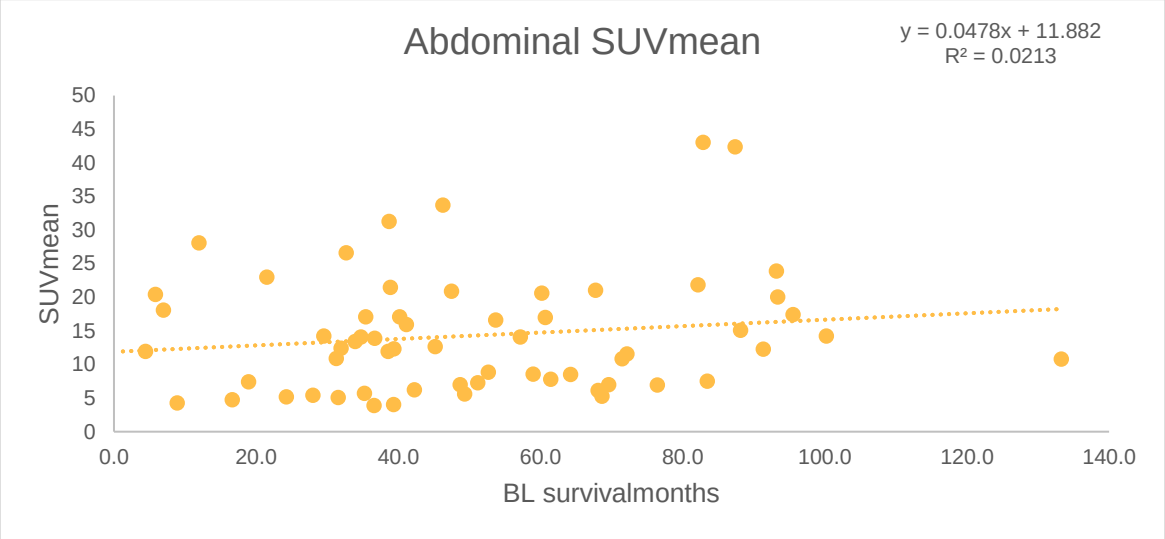

Figure 23: Abdominal SUVmean to BL survival months distribution

Low abdominal tumor volume and prolonged survival months do not show a strong correlation. The trendline of abdominal SUVmean and BL survival months do not show any correlation. The R^2-values for both graphs are low indicating that the distribution does not correlate strongly with the trendline.

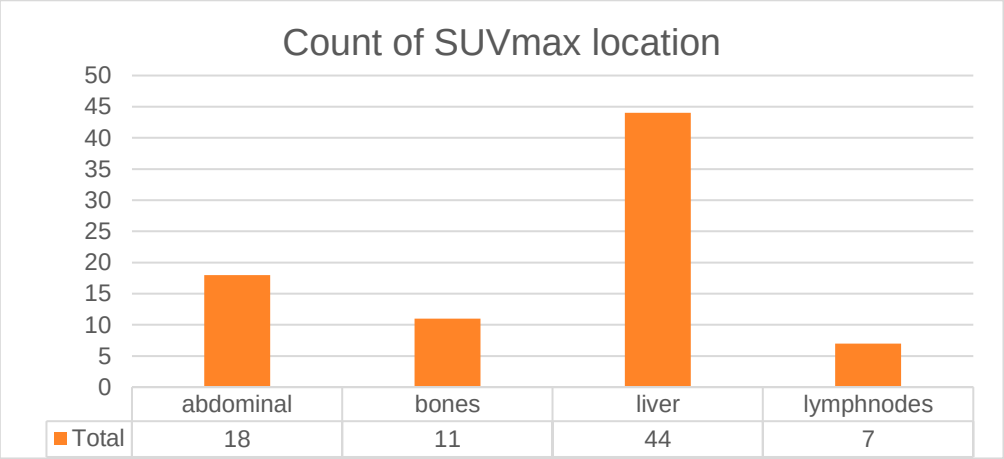

Figure 24: Count of SUVmax location

For 54% of all patients the overall SUVmax was located in the liver. This is because the liver also has a high physiological ^{68}Ga-DOTATOC uptake. The high liver SUVs caused the thresholding issues, mentioned previously in the methods.

3.2 Univariate Cox Regression results

Table 4: Univariate cox regression - BL PET/CT imaging parameters

Parameter	N	Deceased	HR (95% CI for HR)	P-value z Pr(>|z|)
Total tumor volume (TTV)	81	**46**	**1.001 (0.9998-1.001)**	**0.122**
Bone tumor volume (BTV)	40	23	1.001 (0.9981-1.003)	0.557
Liver tumor volume (LTV)	73	43	1.001 (0.9997-1.001)	0.228
Lymph node tumor volume (LNTV)	41	25	1.008 (0.9945-1.023)	0.236
Abdominal tumor volume (ATV)	62	35	1.014 (1.003-1.025)	0.0162*
Total SUVmean	**80**	**45**	**0.9748 (0.9319-1.02)**	**0.267**
Bone SUVmean	40	23	0.9447 (0.8791-1.015)	0.121
Liver SUVmean	72	42	0.9634 (0.9155-1.014)	0.152
Lymph node SUVmean	40	24	0.9958 (0.9273-1.069)	0.907
Abdominal SUVmean	61	34	0.9963 (0.9598-1.034)	0.845
Total SUVmax	**80**	**45**	**0.987 (0.9695-1.005)**	**0.151**
Bones SUVmax	40	23	0.977 (0.9493 -1.005)	0.112
Liver SUVmax	72	42	0.9939 (0.9754 -1.013)	0.523
Lymph nodes SUVmax	40	24	0.9984 (0.9639-1.034)	0.93
Abdominal SUVmax	61	34	0.9941 (0.9756-1.013)	0.541

The total tumor volume, as well as the tumor volume per organ system were analyzed via univariate cox regression with the primary endpoint being overall survival as of the BL PET/CT. TTV, BTV, LTV and LNTV had a hazard ratio (HR) of 1 and had non-significant p-

values, thus without prognostic relevance. ATV had an HR of 1.014 with a significant p-value ($p<0.05$), which may point toward a survival advantage for patients with low ATV.

Total SUVmean and SUVmax as well as the SUVmean/max per organ system had an HR of slightly below 1, with non-significant p-values, thus without prognostic relevance.

Table 5: Univariate cox regression - BL PET/CT descriptive parameters

Parameter	N	Deceased	HR (95% CI for HR)	P-value z Pr(>|z|)
Sex	81	46	0.5718 (0.3034-1.078)	0.0839
Functionality	65	37	0.8164 (0.4045-1.648)	0.571
Ki67	57	35	1.018 (0.956-1.085)	0.571
Amount of organ systems affected	81	46	0.9931 (0.7201- 1.37)	0.966

The descriptive parameters yielded non-significant results. The Sex had an HR of 0.57 with a p-value of 0.08, showing that women may have a survival advantage.

Table 6: Univariate cox regression - BLFU PET/CT imaging parameters

Parameter	N	Deceased	HR (95% CI for HR)	P-value z Pr(>|z|)
Log diff Total tumor volume (diffTTV)	50	28	0.565 (0.2997-1.065)	0.0775
Log diff Bone tumor volume (diffBTV)	26	18	1.046 (0.9802-1.117)	0.174
Log diff Liver tumor volume (diffLTV)	47	27	0.8697 (0.7776-0.9727)	0.0145*
Log diff Lymph node tumor volume (diffLNTV)	28	19	0.9342 (0.8845-0.9866)	0.0145*
Log diff Abdominal tumor volume (diffATV)	42	24	0.9742 (0.9159-1.036)	0.408
Log diff Total SUVmean	49	27	0.9035 (0.4305-1.896)	0.788
Log diff Total SUVmax	49	27	1.294 (0.6476-2.588)	0.465

The total tumor volume reduction or growth between the BL PET/CT and the FU PET/CT were analyzed via univariate cox regression with the primary endpoint being overall survival as of the FU PET/CT. The difference was converted logarithmically for a relative representation of the tumor volume difference. Positive values therefore represented a decrease in tumor volume, whereas negative values represented an increase in tumor volume.

The TTV difference had an HR of 0.565 with a non-significant p-value of 0.078. Even with the result being non-significant, the result could still point to a survival advantage for total tumor reduction.

A reduction of liver tumor volume had an HR 0.87 with a significant p-value of 0.0145, which may point towards a survival advantage for liver tumor reduction. Lymph node tumor reduction had an HR 0.93 ($p = 0.0145$). A survival advantage is less likely than for the liver tumor reduction, as the HR is closer to 1.

The remaining organ systems had non-significant p-values with HR close to 1, thus without prognostic relevance.

Fluctuations in the total SUVmean and SUVmax also yielded non-significant results.

3.3 Multiple Cox regression results

Table 7: Multiple Cox regression - BL PET/CT

Parameter	N	HR (95% CI for HR)	P-value (>|z|)
VOL	44	1.000 (0.9990-1.0013)	0.806952
abdominalVOL		1.030 (1.0146-1.0460)	0.000131 ***
sex		0.314 (0.1036-0.9518)	0.040633 *
functionality01		1.300 (0.4778-3.5393)	0.607044
Ki67		1.124 (1.0104-1.2514)	0.031558 *

The multiple cox regression of TTL, abdominal TL, sex, functionality of tumor, ki67 yielded significant results for the abdominal tumor load (p=0.00013), sex (p=0.04) and ki67(p=0.03). The abdominal TL (HR=1.03) and Ki67 (HR=1.124) both are unfavorable to overall survival, whereas the female sex (HR=0.3) had a favorable effect on overall survival.

3.4 Survival curves among patient subgroups via Kaplan-Meier graphs

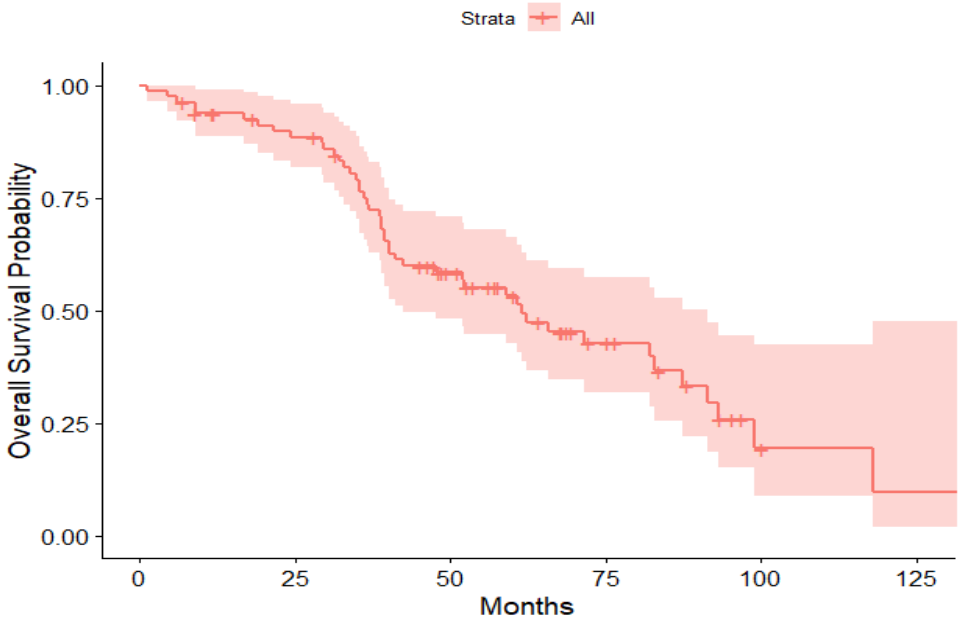

Figure 25: KM - Overall survival of patient collective

The median survival time was 47.5 months measured as of the BL PET/CT. Out of the 81 patients 48 deceased during the follow-up period.

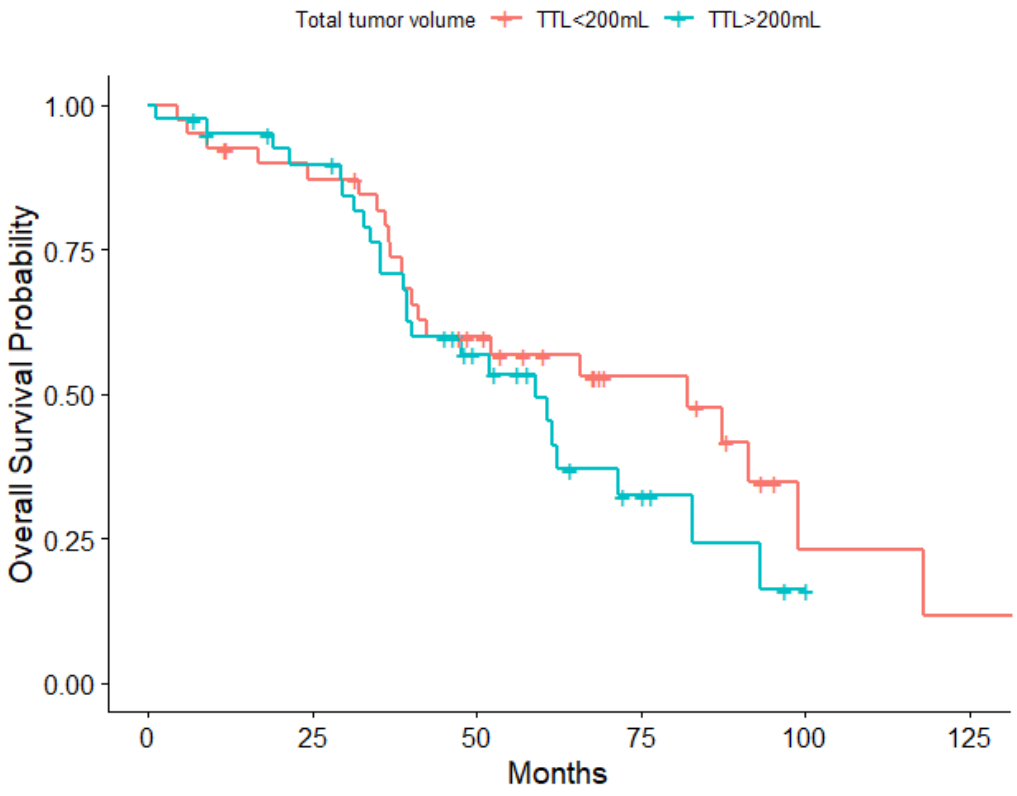

Figure 26: KM - Total tumor load, survival advantage of <200mL at BL PET/CT

Total tumor volume was divided into two groups, by using the median tumor volume (201.27 mL) as a reference. Patients with a total tumor volume of below 200 mL (n = 40, deceased = 22) had a median survival time of 50 months as of the BL PET/CT. Patients with a total tumor volume above 200 mL (n = 41, deceased = 24) had a median survival time of 46.3 months as of BL PET/CT.

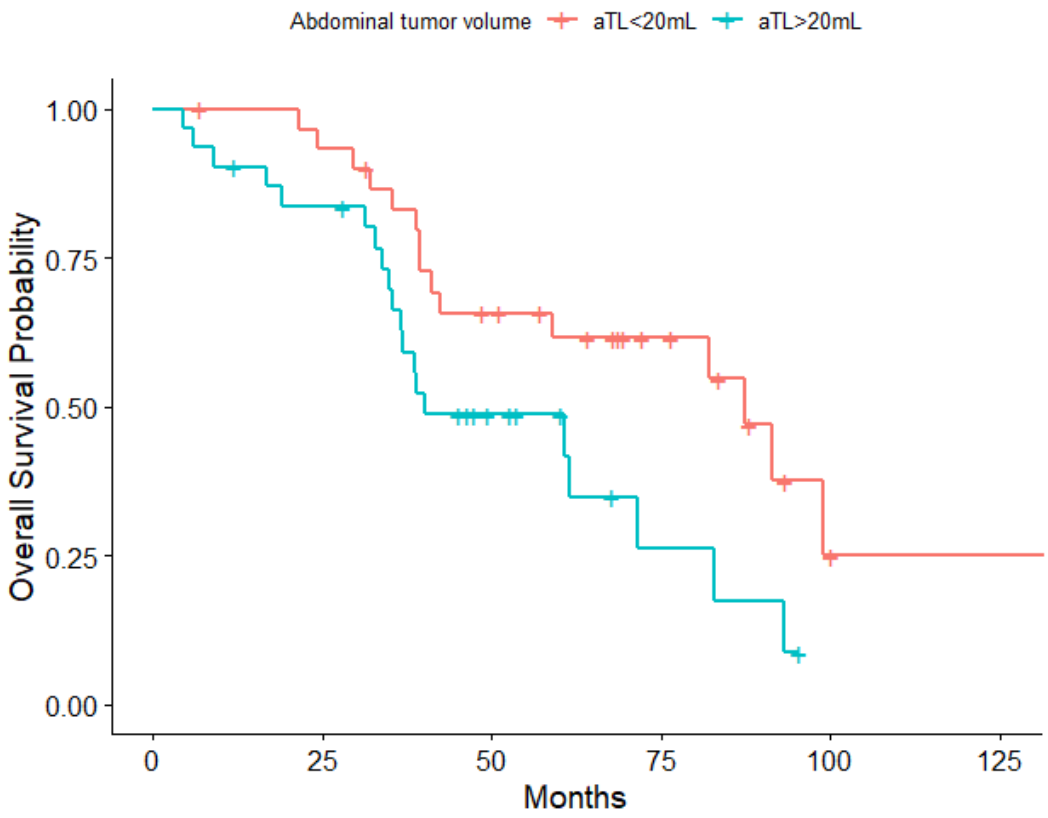

Figure 27: KM - Abdominal tumor load, survival advantage <20 ML at BL PET/CT

Abdominal tumor volume was divided into two groups, by using the median abdominal tumor volume (19.56 mL) as a reference. Patients with an abdominal tumor volume of below 20 mL (n = 31, deceased = 15) had a mean survival time of 59 months as of the BL PET/CT. Patients with an abdominal tumor volume above 20 mL (n = 31, deceased = 20) had a median survival time of 38.7 months as of BL PET/CT.

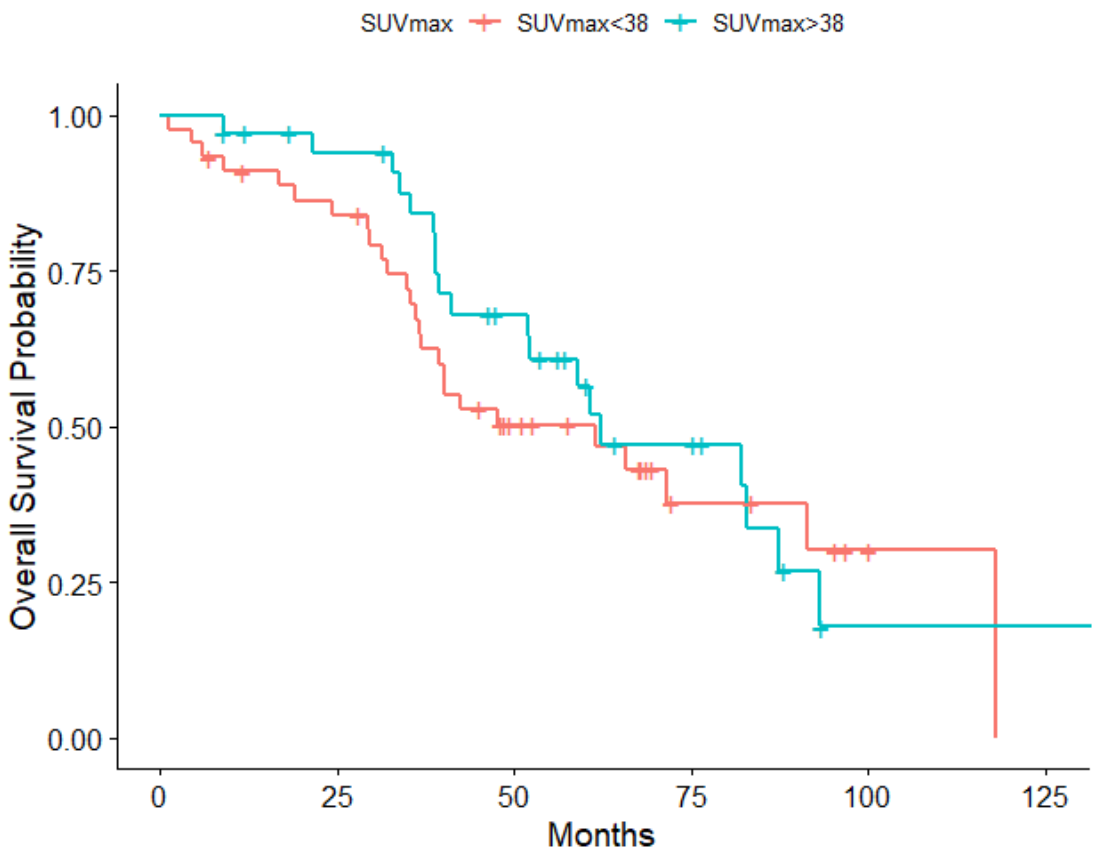

Figure 28: KM - SUVmax, possible survival advantage at >38 SUV, comparison to Ambrosini et al.

SUVmax was divided into two groups, by using the median SUVmax (38.19) as a reference. The results from Ambrosini et al. [48], found a survival advantage for patients with SUVmax >38. However, in our patient collective no survival advantage was detected for patients with a SUVmax of above 38, as can be seen by the overlap of the curves.

For patients with an SUVmax above 38 the median survival time was 52.1 months (n = 35, deceased = 19) as of the BL PET/CT. Patients with a SUVmax below 38 had a median survival time of 42.3 months (n = 45, deceased = 26) as of BL PET/CT.

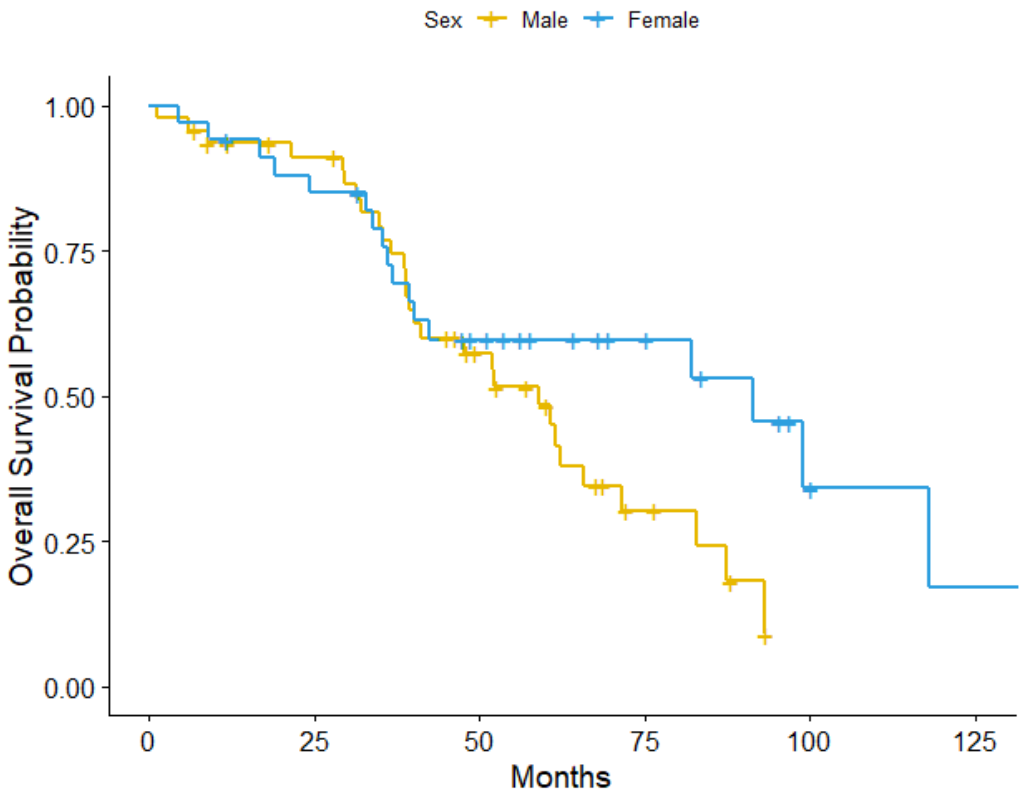

Figure 29: KM - Sex, possible survival advantage of female sex at BL PET/CT

The female sex had a median survival of 50 months (female n = 34, deceased = 17), whereas the male sex had a median survival of 46.3 months (male n = 47, deceased = 29), showing a slight survival advantage for the female sex.

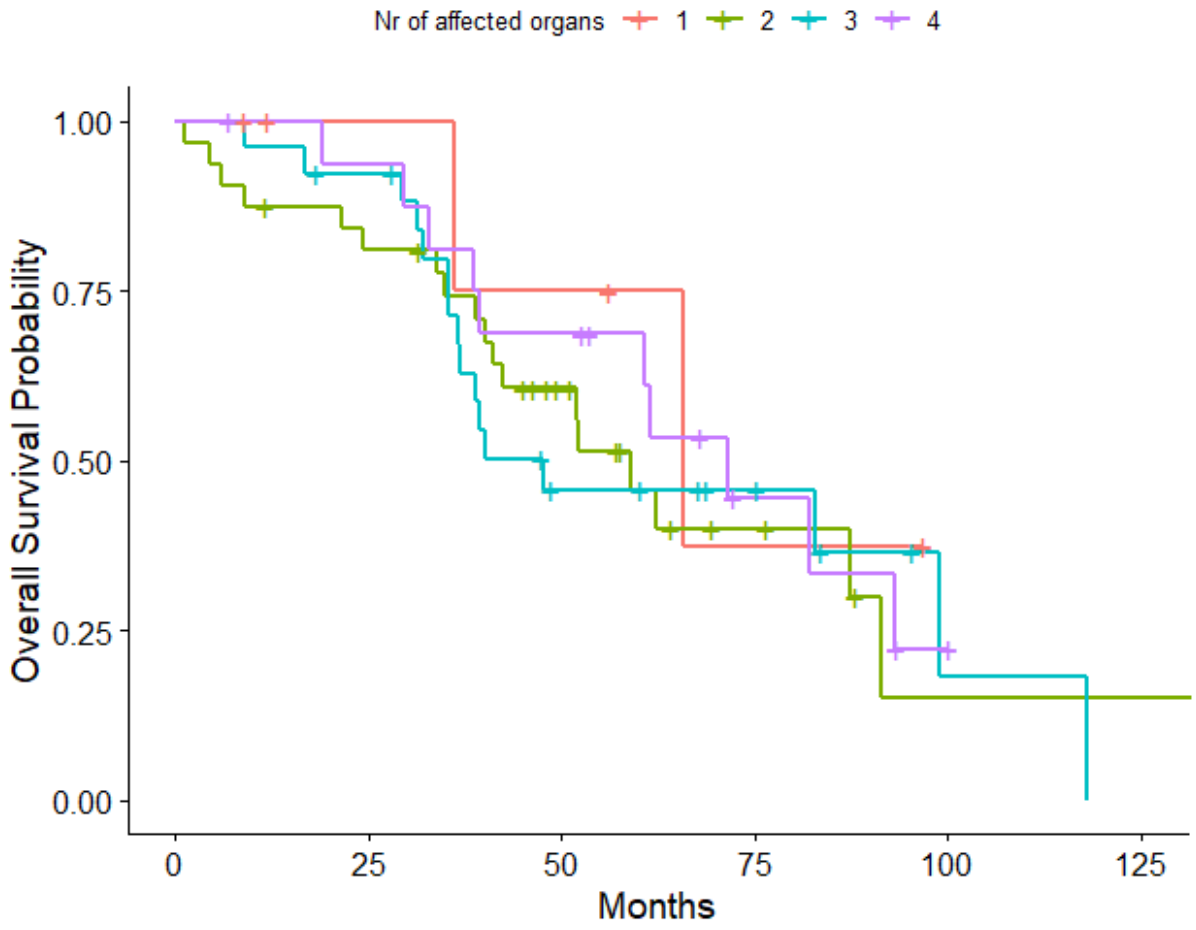

Figure 30: KM - Nr of affected organs 1 - 4 survival analysis

The patient collective was divided into 4 subgroups depending on the number of organ systems affected by the cancer. Patients with 1, 2, 3, or 4 affected organs were plotted against each other to see if the spread, to analyze survival advantage. No survival advantage was detected for spread of cancer. (**1 organ**: n = 6, deceased = 2; **2 organs**: n= 32, deceased = 18; **3 organs**: n = 26, deceased = 16; **4 organs**: n = 17, deceased = 10).

4 Discussion

4.1 Results summarized

In addition to the automatic segmentation, manual segmentation had to be performed for 2.5% of all lesions, thus in only few cases profound expertise is necessary to classify lesions. The median overall survival (OS) was 50.7 months, median total tumor volume (TTV) was 201.27 mL, median liver TV (LTV) was 165.34mL, median abdominal TV (ATV) was 12.93 mL.

The abdominal TV, although low in comparison to the total tumor volume, may be prognostically unfavorable with a Hazard Ratio (HR) of 1.014 (p=0.016) in the univariate cox regression, whereas TTV, LTV, BTV and LNTV had an HR of close to 1 with non-significant p values. The analysis of the follow up PET/CTs showed that the reduction of liver tumor volume had a HR of 0.87 (p=0.015) and the reduction of lymph node tumor volume had a HR of 0.93 (p=0.015) in the univariate cox regression. The total tumor volume reduction had a HR of 0.57 (p=0.078) in the univariate cox regression.

SUVmean and SUVmax did not have a prognostic impact in this study. With the HR close to one no potential trend could be observed.

The multiple cox regression yielded significant results for the abdominal tumor volume (p=0.00013), sex (p=0.04) and ki67(p=0.03). ATV (HR=1.03) and Ki67 (HR=1.124) are both unfavorable to overall survival, whereas the female sex (HR=0.3) had a favorable effect on OS. Especially abdominal tumor load shows a more pronounced result in the multiple cox regression. This shows that the influence of other parameters does not seem to affect the prognostic impact of ATV.

Total tumor volume, the amount of organ systems affected, and the functionality of the tumor did not show a prognostic impact in this study.

4.2 Volume correlation with OS

FDG PET/CTs are the most studied tracer when it comes to the analysis of imaging data and its prognostic impact, which is why even when researching other tracers, the results of FDG studies are often referenced.

Standardized interpretation procedures have been studied extensively for FDG PETs resulting in the development of the PET Response Criteria in Solid Tumors (PERCIST) [44] and many different types of quantifying methods that are based on these criteria [39]. This has resulted in a multitude of studies showing that quantitative values derived from metabolic imaging can range from having significant prognostic value [4, 17] or none at all [45], when assessing the overall survival, disease progression or therapy response in cancer patients.

There have also been studies focusing on the quantification of prostate specific membrane antigen (PSMA) uptake in PET/CTs for prostate cancer. In the study by Seifert et al. it was found that the tumor volume had a high correlation with the overall survival in patients suffering from advanced prostate cancer that received Lu-PSMA-617 therapy [3]. This study as well as Pinochet et al. [42] also showed that manual segmentation had a high correlation with semi-automatic segmentation, which further supported the decision to use AI assisted programs, specifically CNNs, to conduct the quantification of the PET/CTs.

As explained in the introduction, the importance and prognostic impact of the quantification of SSTR tracer accumulation is still unclear. For NETs it has already been proven that the metabolic tumor volume (MTV) determined in FDG PET/CTs is an independent prognostic factor for overall survival [17]. This is attributed to the more aggressive tumor phenotype associated with FDG positivity. A study by Ohnona et al. investigating the tumor volume acquired through ^{68}Ga-DOTATOC-PET/CT, found that pancreatic NET patients with a tumor volume >14 cm^3 had a higher risk of disease progression within two years [2].

The results of the study by Ohnona et al. pointed towards the assumption that ^{68}Ga-DOTATOC derived tumor mass calculation could have a significant correlation with the overall survival of NET patients. In contrast, our results showed that the volume derived from the BL PET/CT did not have a significant correlation with the overall survival. These differing results from the previously mentioned pNET study by Ohnona et al. may be due to the chosen patient collective, as patients with NETs of any primary were included in the study. Other differences include the stage of the disease at point of inclusion, as well as previously undergone therapies. The patients in this study were in the end-stages of their cancer and had already undergone multiple therapy options. The total tumor load median for our patient collective was 201.27 mL, with only 2 patients out of the entire collective having tumor burdens lower than 14 mL. This is a stark contrast to the patient collective by Ohnona, as their median tumor volume was 22.8 mL for stage III/IV NETs and 3.2 mL for stage I/II NETs. Ohnona et al. chose patients who had not yet received SSAs or other first-line therapies and therefore could have a different SSTR expression. The expression of SSTR can fluctuate throughout therapy which may affect the prognostic ability of SSTR-PET/CTs. Organ-specific segmentation seemed to have more promising results but will be discussed separately in the chapter “Organ-specific tumor quantification and its correlation to OS”.

So far there are few studies investigating the volume difference calculated from SSA-tracer accumulation as a prognostic parameter, as generally a reduction in tumor size in itself is considered a sign of regression or positive therapy response (PERCIST) [44].

The expression of SSTR however does not have to directly correlate to the tumor size, as the expression of receptors may vary throughout the cancerous tissue, depending on changes in the grading and/or in the SSTR status [49]. As the patients chosen for this study all showed a high SSTR expression, SSTR expression is considered to represent the actual anatomical tumor margins for this study. We concluded that the total tumor difference could show that a decrease in tumor volume may positively affect the overall survival, this result was non-significant but may simply require a bigger patient collective.

4.3 SUVmax/SUVmean correlation with OS

The standardized uptake value of PET/CTs is an interesting parameter, that has become the focus of many studies investigating imaging parameters. In ^{18}FDG-PET/CTs a high tracer uptake is associated with high tumor aggressiveness [25].
Due to high SUVs in ^{18}FDG PET/CTs being a marker of tumor aggressiveness, many studies have found that a correlation of prognosis and SUVmax or SUVmean exist, e.g., the study by Im et al. showing a correlation of SUVmax and overall survival for pancreatic cancer [4]. A study by Bahri et al. investigated SUV ratios in ^{18}FDG PET/CTs of NETs and documented a negative prognostic impact for high ratios [50].

For SSTR-PET/CTs there are fewer studies available concerning the prognostic impact of SUVs. It has been shown that SSTR positive patients have a better prognosis than SSTR negative patients [51] as, for example, the therapeutic options have a bigger impact in prolonging life. It is therefore plausible to believe that high SUVs in SSTR PET/CTs may also have a positive prognostic impact for NET patients.
A study from Ambrosini et al. [48] investigating pancreatic NETs found that a SUVmax of smaller than 38 was a risk factor for progression free survival. Another study by Sharma et al. found similar results with a high SUVmax being a positive prognostic factor, superior even to SUVmax measured in ^{18}FDG-PET/CTs [52]. In both studies the PET/CTs were conducted with the tracer ^{68}Ga-DOTANOC, which has a slightly different receptor affinity, compared to DOTATOC [22].

In this study there was no correlation detected between SUVmax, SUVmean and overall survival. The univariate cox regression yielded hazard ratios close to 1 with non-significant p-values. It was also attempted to reproduce the results by Ambrosini et al. with DOTATOC instead of DOTANOC. The patient collective was divided into two subgroups with SUVmax below and above 38. The Kaplan-Meier survival curve showed that the patient collective >38 SUVmax had a longer survival time as of BL PET/CT up until 75 months. After 75 survival months there did not seem to be a clear advantage. However, these results are non-significant.
We can therefore conclude that the total SUVmax/mean as well as the organ-specific values

do not have a prognostic impact, contrary to the results of the above-mentioned studies. A significant correlation might be detected in a bigger or more homogenous patient collective.

4.4 Organ-specific tumor quantification and its correlation to OS

There have been few studies on organ-specific quantification and correlating prognosis, specifically for ^{68}Ga-DOTATOC PET/CTs. There are however some studies, that have used the organ-specific segmentation technology for other areas. For example, a study by Pace et al. investigated the difference between PET/CT and PET/MRI for lesion detection in breast cancer patients [53]. The lesion quantification distinguishes between the primary tumors, lymph nodes and distant metastases – however, this was a comparative study between CT and MRI and the correlation to overall survival was not investigated for the individual organ systems. It does however demonstrate that organ-specific quantification is more in line with the individualized therapeutic approach to cancer treatment and with the support of CNNs is more easily applicable in routine clinical procedures.

In this study the majority of the measured tumor mass was located in the liver averaging at 248.04 mL, the extra hepatic tumor mass averaged around 20-60 mL, in other words on average only a tenth of the total tumor volume. Due to the difference in magnitude, symptoms caused by invasivity may be hard to compare. The liver can compensate a large amount of cancerous tumor burden without decompensating. In this study, a high liver tumor load measured at the BL PET/CT did not seem to have a significant effect on overall survival. However, the liver tumor reduction, averaging at 44.09 mL, showed a significant positive prognostic effect (HR 0.87, p = 0.0145). These results support the usage of locally ablative procedures, such as transcatheter arterial chemoembolization (TACE) or radioembolization, to reduce liver tumor burden even in the end stage of the disease. From a clinical perspective reduction of liver tumor mass also helps reduce clinical symptoms especially in low-grade NENs [54].

In contrast to the liver metastases, mesenterial and peritoneal tumor manifestation typically cause severe complications in earlier stages, such as bowel obstruction, perforation, bleeding, or ischemia. Therefore, a reduction in mesenterial tumor mass through surgery has been shown to prolong survival [55, 56]. In this study a high abdominal tumor load measured at the BL PET/CT may be associated with a negative effect on the overall survival (HR = 1.014, p = 0.0162), this effect may be more pronounced in a greater patient collective.
In the Kaplan-Meier survival curve the patient collective was divided into two subgroups; patients with <20 mL of abdominal tumor mass and patients with >20mL of abdominal tumor mass measured at the BL PET/CT. The graph shows that patients with an abdominal tumor mass under 20 mL have a survival advantage, this result also had a significant p-value (p=0.026).

Interestingly no significant effect was shown in the tumor reduction of abdominal tumor mass (on average 6.72 mL), in this case it may also be due to the small patient collective. Another aspect that must be considered, is that the patient collective is in the end stage of their disease - therefore an abdominal tumor reduction might not have the same effect as for patients in the early stages of their disease. One may conclude that abdominal tumor mass should be removed as early as possible to achieve a survival advantage.

Another interesting observation of this study is the reduction of lymph nodal tumor mass (HR = 0.93, p= 0.0145). The reduction may have a slight positive prognostic effect for overall survival. On average the reduction of lymph nodal tumor mass amounts to 4.33 mL. As this is quite a low volume and the HR is close to 1, one could conclude that this effect is too small to have any kind of prognostic power. Thus, the therapeutic effect of PRRT is dominant in liver metastasis.

The remaining organ systems did not have significant results and it would need larger patient cohorts to either confirm the prognostic value of tumor reduction after PRRT also in other organ systems or to stratify for different distribution patterns of metastasis as manifestation of different biological behavior

4.5 Study Limitations

There are certain limitations that must be considered in this study. One issue presented itself in the heterogeneity of the patient collective. Mostly patients with a grading of G1-G2 were selected, however there were 3 patients (of which it had been documented) that had already progressed to G3. Due to G3 NETs generally being poorly differentiated it can lead to a reduced expression of SSTR, thereby leading to a false decrease in tumor size [49]. Another factor that needs to be considered concerning the patient heterogeneity, is the origin of the NET as well as the therapies the patients had undergone before receiving PRRT. SSAs may change the expression of SSTR of the tumor

Another issue is that the patient collective may be too small to determine the true prognostic power of these imaging parameters. For most parameters the hazard ratio was close to 1 meaning that a survival advantage is not detectable. A bigger patient collective could lead to more impactful values.

It is important to note that competing causes of death, in other words non-NET related deaths may also have impacted the prognostic power of this study. According to Low et al. competing causes of death make up 42.5% of the mortality causes in NET patients [57]. This observation was made using the Surveillance, Epidemiology, and End Results database (SEER) by analyzing 29,981 NET patients. This relatively high non-NET mortality is partly explained by the life-prolonging therapeutic options having greatly advanced in the past

decade, as well the average age being 50-60, meaning that the average NET patient generally has a higher risk of dying of comorbidities.
To circumvent this effect in our study, two patients were censored, due to non-NET related deaths. However, it is unclear if patients with multiple co-morbidities may have had a confounding effect on the survival analysis.

Certain NET primaries have a poorer prognosis than others, specifically rectal NETs having the best prognosis and pancreatic NETs having the highest risk of mortality [58]. In this study no significant difference in overall survival was observed between the different primary sites. This is most likely explained due to the small patient collective and the overrepresentation of intestinal and pancreatic NETs.

Among NET patients the functionally active tumors are usually associated with a poorer prognosis than patients with non-active tumors. In this study functionality of tumor was not associated with a higher overall survival. This may be because the patient collective is too small, however for many patients the functionality was difficult to determine. This is because NET patients often have diffuse abdominal symptoms such as abdominal pain and/or diarrhea. This may be caused by excessive hormone production of functionally active tumors or due to previous therapies such as bowel-removal procedures. The invasive nature of a non-active tumor could also lead to such symptoms. Therefore, the functionality was difficult to determine for all patients, hence yielding unclear results [59].

Segmentation issues included the correct quantification of liver tumor mass, due to physiological tracer accumulation. This issue can lead to an overestimation of liver tumor mass. Other issues consisted of the inclusion of physiological intestinal tracer accumulation as mesenterial metastases or the involvement of the adrenal glands in the liver tumor mass, due to the proximity of the organs. The relatively high cut-off SUV of 4 may also have led to an underestimation of non-hepatic tumor mass, as there were some visible non-hepatic lesions that were not included in the segmentation with a SUVmax lower than 4.

5 Conclusions

This study may encourage further investigation into the imaging parameters of SSTR-PET/CTs in larger patient cohorts and has shown ^{68}Ga-DOTATOC derived tumor volume may give additional prognostic information and could aid physicians in making more individualized therapeutic decisions for NET patients. Especially abdominal tumor volume seemed to have the biggest prognostic significance. This may be because abdominal tumor load can lead to severe complications such as e.g., ileus, pancreatitis, and cholestasis even for low tumor volumes. Liver tumor reduction may also have a positive prognostic effect, which supports the usage of locally ablative procedures to reduce tumor volume.

SUVmax and SUVmean were not prognostically significant but may be interesting when viewed together with SUV values from FDG PET/CTs or when investigating therapy response. These values might also be more significant for patients who have not yet undergone different therapeutic approaches, such as PRRT, and are still in the early stages of their disease. Due to the selection of patients for PRRT according to Somatostatin receptor expression, prognostic effects of SUV values in an unselected cohort might well occur.

As NETs are often discovered in a palliative state due to late clinical presentation, one of the main aims of treating this illness is disease stabilization. Especially the results of abdominal TL and liver TL could point towards the importance of tumor burden reduction, when trying to prolong life. Tumor reduction is also an important consideration when trying to increase the quality of life for the patient. This aspect was not investigated in this study but has been proven to improve quality of life in other studies assessing the impact of tumor burden of NETs [54].

This study specifically investigated different quantifying methods and may help future studies in finding a suitable way for quantifying ^{68}Ga-DOTATOC PET/CTs. This field of technology is constantly growing, and new quantifying methods are constantly being developed, refined, and individualized for specific tracers and cancer types. As this is such a fast-progressing field it will be difficult to introduce standardized methods of quantification, as for certain tracers or cancers it is still unclear what the best approach should be. Hence, the direct comparison of studies using different methods may be difficult and may even lead to different outcomes. On the other hand, as the CNNs become more precise, different algorithms or parameters may play a minor role in the actual outcome; in particular when large patients cohorts are available for validation. The resolution of PETs and CTs also continue to advance and will consequently influence the quantification accuracy of tumor load. Studies investigating different algorithms will continue to specify the best possible approaches to metabolic tumor quantification. The methodology of this study may serve as a

basis for future studies further validating ^{68}Ga-DOTATOC PET/CT derived parameters for neuroendocrine tumors.

6 Summary

Although PET imaging displays outstanding contrast and is therefore well suited for tumor segmentation, few studies have specifically investigated volumetric parameters regarding their prognostic impact on neuroendocrine tumors (NET). In this study the total tumor load (TTL), SUVmean and SUVmax, as well as the tumor load of specific organ systems of NET patients were derived from ^{68}Ga-DOTATOC PET/CTs and correlated to overall survival after PRRT.

Overall, 81 patients treated with PRRT between 2009 to 2016 were included in this study. Tumor volumes were generated from a baseline PET/CT before PRRT via a standardized semi-automatic delineation procedure using PARS Software (v3.0 Siemens). Additionally, out of the entire patient collective, 52 follow up PET/CTs one year after the start of PRRT were analyzed. Total tumor volumes and tumor volumes from liver, bones, lymph-nodes, and abdominal TL (consisting of mesenterial and peritoneal manifestations) as well as SUVmean and SUVmax were analyzed via multivariate and univariate Cox regression.

During the testing phase different algorithms for segmentation, including common methods used for other tracers, as well as creating new DOTATOC-specific algorithms, were assessed in their suitability for conducting this study. The DOTATOC-specific algorithm was evaluated by multiplying different factors with a reference background activity VOI located in the liver and then comparing the generated tumor volumes with tumor volume measurements conducted in the corresponding arterial CT. This way the factor that resulted in the volume that most closely related to the CT measurement could be determined.
Pre-existing patient-specific algorithms used for FDG and PSMA were also tested in their suitability for DOTATOC segmentation. The patient-specific algorithms ended up not being viable options for this study, especially due to time-related inefficiency.

It was found that the fastest and most accurate method was using a universally applicable threshold for segmentation. The selection of lesions was set at a SUVpeak above 4 and delineation occurring at 42% of SUVmax. Lesions with a tumor volume smaller than 0,5 mL were excluded. For evident lesions without available SUVpeak, segmentation was performed manually.

The manual adaption of segmentation had to be performed for 2.5% of all lesions. The median overall survival (OS) was 50.7 months, median total TL was 201.27 mL, median liver TL was 165.34mL, median abdominal TL was 12.93mL. The abdominal TL was prognostically unfavorable with a Hazard Ratio (HR) of 1.014 (p=0.016) in the univariate cox

regression, whereas total TL, liver TL, bone TL and lymph-node TL had an HR of close to 1 with non-significant p values. Analysis of the follow up PET/CT showed that tumor reduction of liver TL had a HR of 0.87 (p=0.015) and the tumor reduction of lymph node TL had a HR of 0.93 (p=0.015) in the univariate cox regression. The total TL reduction had a HR of 0.57 (p=0.078) in the univariate cox regression.

The multivariate cox regression of TTL, abdominal TL, sex, functionality of tumor, ki67 yielded significant results for the abdominal tumor load (p=0.00013), sex (p=0.04) and ki67(p=0.03). The abdominal TL (HR=1.03) and Ki67 (HR=1.124) both are unfavorable to overall survival, whereas the female sex (HR=0.3) had a favorable effect on OS.
The univariate cox regression of abdominal TL measured at BL PET/CT yielded significant results with an unfavorable effect on overall survival. The univariate cox regression also yielded significant results for liver and lymph-node tumor reduction showing a positive prognostic effect.

This study shows that organ-specific tumor segmentation from PET/CTs might result in prognostic parameters in NET patients. In particular abdominal TL might be associated with a shorter overall survival. The effect may be greater with a larger patient collective and a longer follow up period. The reduction of liver TL may have a positive prognostic effect on overall survival which supports the use of ablative procedures reducing liver tumor mass in liver dominant disease. This study also shows the exploration of different segmentation methods as well as demonstrating a viable universally applicable algorithm for ^{68}Ga-DOTATOC segmentation.

7 Zusammenfassung (Deutsch)

Obwohl die PET-Bildgebung einen hervorragenden Kontrast aufweist und daher gut zur Tumorsegmentierung geeignet ist, haben nur wenige Studien volumetrische Parameter hinsichtlich ihrer prognostischen Bedeutung für neuroendokrine Tumoren (NET) spezifisch untersucht. In dieser Studie wurde die Gesamttumorlast (TTL), SUVmean und SUVmax sowie die Tumorlast bestimmter Organsysteme von NET-Patienten aus ^{68}Ga-DOTATOC-PET/CTs abgeleitet und mit dem Gesamtüberleben nach PRRT korreliert.

Insgesamt wurden 81 Patienten, die zwischen 2009 und 2016 mit PRRT behandelt wurden, in diese Studie eingeschlossen. Die Tumorvolumina wurden anhand eines Ausgangs-PET/CT (*baseline*) vor der PRRT über ein standardisiertes semi-automatisches Segmentierungsverfahren unter Verwendung der PARS-Software (v3.0 Siemens) generiert. Zusätzlich wurden aus dem gesamten Patientenkollektiv 52 Follow-Up-PET/CTs ein Jahr nach Beginn der PRRT analysiert. Gesamttumorvolumina und Tumorvolumina aus Leber, Knochen, Lymphknoten und abdominellem Tumor Last (bestehend aus mesenterialen und

peritonealen Metastasen) sowie SUVmean und SUVmax wurden mittels multipler und univariater Cox-Regression analysiert.

Während der Testphase wurden verschiedene Algorithmen zur Segmentierung, einschließlich gängiger Methoden, die für andere Tracer verwendet werden, sowie die Entwicklung neuer DOTATOC-spezifischer Algorithmen auf ihre Eignung für die Durchführung dieser Studie bewertet. Der DOTATOC-spezifische Algorithmus wurde evaluiert, indem verschiedene Faktoren mit einer in der Leber lokalisierten Referenz-Hintergrundaktivitäts-VOI multipliziert wurden, um patientenspezifische Tumorvolumina zu erzeugen. Diese PET Tumorvolumina wurden anschließend mit Tumorvolumenmessungen verglichen, die im entsprechenden arteriellen CT durchgeführt wurden, um den bestmöglichen Faktor zu ermitteln.
Bestehende patientenspezifische Algorithmen, die für FDG und PSMA verwendet werden, wurden ebenfalls auf ihre Eignung für die DOTATOC-Segmentierung getestet. Die patientenspezifischen Algorithmen erwiesen sich jedoch vor allem aufgrund ihrer zeitlichen Ineffizienz als keine praktikable Option für diese Studie.

Es stellte sich heraus, dass die schnellste und genaueste Methode darin bestand, einen universell anwendbaren Schwellenwert für die Segmentierung zu verwenden. Die Auswahl der Läsionen wurde auf einen SUVpeak über 4 eingestellt und die Abgrenzung erfolgte bei 42 % des SUVmax. Läsionen mit einem Tumorvolumen kleiner als 0,5 ml wurden ausgeschlossen. Bei offensichtlichen Läsionen ohne verfügbaren SUVpeak wurde die Segmentierung manuell durchgeführt.

Zusätzlich zur automatischen Segmentierung, musste bei 2,5 % aller Läsionen eine manuelle Segmentierung durchgeführt werden. Das mediane Gesamtüberleben (*overall survival* - OS) betrug 50,7 Monate, die mediane Gesamttumorlast (*total tumor load* - TTL) betrug 201,27 ml, die mediane Leber-TL betrug 165,34 ml, die mediane abdominale TL betrug 12,93 ml. Die abdominale TL war mit einer Hazard Ratio (HR) von 1,014 (p = 0,016) in der univariaten Cox-Regression prognostisch ungünstig, während Gesamt-TL, Leber-TL, Knochen-TL und Lymphknoten-TL eine HR von nahe 1 nicht- signifikante p-Werte aufwiesen. Die Analyse der Nachsorge zeigt, dass die Tumorreduktion von Leber-TL eine HR von 0,87 (p = 0,015) und die Tumorreduktion von Lymphknoten-TL eine HR von 0,93 (p = 0,015) in der univariaten Cox-Regression aufwiesen. Die Gesamt-TL-Reduktion hatte eine HR von 0,57 (p = 0,078) in der univariaten Cox-Regression.

Die multiple Cox-Regression von TTL, abdominaler TL, Geschlecht, Tumorfunktion, ki67 ergab signifikante Ergebnisse für die abdominale Tumorlast (p=0,00013), Geschlecht (p=0,04) und ki67 (p=0,03). Die abdominale TL (HR=1,03) und Ki67 (HR=1,124) sind beide ungünstig für das Gesamtüberleben, während das weibliche Geschlecht (HR=0,3) einen

günstigen Effekt auf das Gesamtüberleben hatte.
Die univariate Cox-Regression der abdominellen TL, gemessen bei BL-PET/CT, ergab signifikante Ergebnisse mit ungünstigem Einfluss auf das Gesamtüberleben. Die univariate Cox-Regression lieferte ebenfalls signifikante Ergebnisse für die Reduktion von Leber- und Lymphknotentumoren, die einen positiven prognostischen Effekt zeigten.

Diese Studie zeigt, dass die organspezifische Tumorsegmentierung von PET/CTs zu prognostischen Parametern bei NET-Patienten führen könnten. Insbesondere abdominelle TL könnte mit einem kürzeren Gesamtüberleben assoziiert sein. Der Effekt könnte bei einem größeren Patientenkollektiv und einer längeren Nachbeobachtungszeit ausgeprägter sein. Die Reduktion der Leber-TL könnte einen positiven prognostischen Effekt auf das Gesamtüberleben haben. Dies unterstützt zusätzlich den Einsatz von lokal-ablativen Verfahren, wie z.B. TACE oder Radioembolisation, vor allem bei größtenteils hepatischem Befallsmuster. Diese Studie zeigt ebenfalls die Erforschung verschiedener Segmentierungsmethoden und demonstriert einen praktikablen, universell anwendbaren Algorithmus für die ^{68}Ga-DOTATOC-Segmentierung.

8 Note of thanks

I would like to convey my sincere gratitude to my doctoral supervisor __ for the immense support, patience, and valuable guidance I received for my thesis. I would also like to thank __ the director of the nuclear medicine department of the University Clinic of Mainz for the support and opportunity to conduct this study and write my thesis in his department.

I would like to thank the employees of the nuclear medicine department of the University Clinic of Mainz for their support and assistance. I would also like to express thanks to the employees of the IMBEI institute of the University of Mainz for their aid in the statistical analysis of this study. A special thanks goes to ___, the technical support of PARS, for his assistance in all technical matters.

In addition, I would like to thank my family and friends for their counsel and constant support. I would especially like to thank my colleague ___, as I greatly enjoyed working with you and am deeply grateful for all your help and support.

9 CV

10 Pictures from external sources

- Fig. 1 - Diagram showing the parts of the body neuroendocrine tumours most commonly develop in by Cancer Research UK uploader, 13 January 2016, CC by 4.0 license [60]
    - Image edit based on image from Peptide Receptor Radionuclide Therapy for Neuroendocrine Tumors by Janet Pollard MD, M. Sue O'Dorisio MD, PhD, Thomas O'Dorisio MD & Yusuf Menda MD [61]
- Fig. 2 - Self-made, concept based on therapy scheme from Pavel et al. 2016 ENETS [20]
- Fig. 3 - Nicolas Marincek, Ann-Catherine Jörg, Philippe Brunner, Christian Schindler, Michael T Koller, Christoph Rochlitz, Jan Müller-Brand, Helmut R Maecke, Matthias Briel and Martin A Walter - "Somatostatin-based radiotherapy with [90Y-DOTA]-TOC in neuroendocrine tumors: long-term outcome of a phase I dose escalation study". Journal of Translational Medicine 11 (17). DOI:10.1186/1479-5876-11-17. PMC: 3561188., CC by 2.0 license
- Fig. 9 – E. Poletaev et al. 2016, Artificial neural network for bubbles pattern recognition on the images. Journal of Physics Conference Series. 754 072002, CC by 3.0 license

11 References

1. Griffeth, L.K., *Use of PET/CT scanning in cancer patients: technical and practical considerations.* Proc (Bayl Univ Med Cent), 2005. **18**(4): p. 321-30.
2. Ohnona, J., et al., *Prognostic value of functional tumor burden on 68Ga-DOTATOC PET/CT in patients with pancreatic neuro-endocrine tumors.* Neoplasma, 2019. **66**(1): p. 140-148.
3. Seifert, R., et al., *Semiautomatically Quantified Tumor Volume Using (68)Ga-PSMA-11 PET as a Biomarker for Survival in Patients with Advanced Prostate Cancer.* J Nucl Med, 2020. **61**(12): p. 1786-1792.
4. Im, H.J., et al., *Prognostic Value of Metabolic and Volumetric Parameters of Preoperative FDG-PET/CT in Patients With Resectable Pancreatic Cancer.* Medicine (Baltimore), 2016. **95**(19): p. e3686.
5. Cheebsumon, P., et al., *Assessment of tumour size in PET/CT lung cancer studies: PET- and CT-based methods compared to pathology.* EJNMMI Res, 2012. **2**(1): p. 56.
6. van Loon, J., et al., *Microscopic disease extension in three dimensions for non-small-cell lung cancer: development of a prediction model using pathology-validated positron emission tomography and computed tomography features.* Int J Radiat Oncol Biol Phys, 2012. **82**(1): p. 448-56.
7. Geijer, H. and L.H. Breimer, *Somatostatin receptor PET/CT in neuroendocrine tumours: update on systematic review and meta-analysis.* Eur J Nucl Med Mol Imaging, 2013. **40**(11): p. 1770-80.
8. Chai, S.M., I.S. Brown, and M.P. Kumarasinghe, *Gastroenteropancreatic neuroendocrine neoplasms: selected pathology review and molecular updates.* 2018. **72**(1): p. 153-167.
9. Knigge, U., et al., *ENETS Consensus Recommendations for the Standards of Care in Neuroendocrine Neoplasms: Follow-Up and Documentation.* Neuroendocrinology, 2017. **105**(3): p. 310-319.
10. Klimstra, D.S., et al., *The pathologic classification of neuroendocrine tumors: a review of nomenclature, grading, and staging systems.* Pancreas, 2010. **39**(6): p. 707-12.
11. Breitling, L.P., A. Rinke, and T.M. Gress, *[Gastroenteropancreatic neuroendocrine tumors].* Dtsch Med Wochenschr, 2019. **144**(21): p. 1509-1521.
12. Gockel, I., et al., *[Differentiated surgical therapy for neuroendocrine tumours (NET) of the stomach].* Zentralbl Chir, 2010. **135**(3): p. 203-9.
13. Partelli, S., et al., *ENETS Consensus Guidelines for Standard of Care in Neuroendocrine Tumours: Surgery for Small Intestinal and Pancreatic Neuroendocrine Tumours.* Neuroendocrinology, 2017. **105**(3): p. 255-265.
14. Rinke, A., et al., *Placebo-controlled, double-blind, prospective, randomized study on the effect of octreotide LAR in the control of tumor growth in patients with metastatic neuroendocrine midgut tumors: a report from the PROMID Study Group.* J Clin Oncol, 2009. **27**(28): p. 4656-63.
15. Nilica, B., et al., *Direct comparison of (68)Ga-DOTA-TOC and (18)F-FDG PET/CT in the follow-up of patients with neuroendocrine tumour treated with the first full peptide receptor radionuclide therapy cycle.* Eur J Nucl Med Mol Imaging, 2016. **43**(9): p. 1585-92.
16. Kayani, I., et al., *A comparison of 68Ga-DOTATATE and 18F-FDG PET/CT in pulmonary neuroendocrine tumors.* J Nucl Med, 2009. **50**(12): p. 1927-32.
17. Kim, H.S., et al., *Prognostic Value of Volume-Based Metabolic Parameters Measured by (18)F-FDG PET/CT of Pancreatic Neuroendocrine Tumors.* Nucl Med Mol Imaging, 2014. **48**(3): p. 180-6.
18. Pavel, M., et al., *Gastroenteropancreatic neuroendocrine neoplasms: ESMO Clinical Practice Guidelines for diagnosis, treatment and follow-up.* Ann Oncol, 2020. **31**(7): p. 844-860.
19. Caplin, M.E., et al., *Lanreotide in metastatic enteropancreatic neuroendocrine tumors.* N Engl J Med, 2014. **371**(3): p. 224-33.

20. Pavel, M., et al., *ENETS Consensus Guidelines Update for the Management of Distant Metastatic Disease of Intestinal, Pancreatic, Bronchial Neuroendocrine Neoplasms (NEN) and NEN of Unknown Primary Site.* Neuroendocrinology, 2016. **103**(2): p. 172-85.
21. Strosberg, J., et al., *Phase 3 Trial of (177)Lu-Dotatate for Midgut Neuroendocrine Tumors.* N Engl J Med, 2017. **376**(2): p. 125-135.
22. Pauwels, E., et al., *Somatostatin receptor PET ligands - the next generation for clinical practice.* Am J Nucl Med Mol Imaging, 2018. **8**(5): p. 311-331.
23. Romer, A., et al., *Somatostatin-based radiopeptide therapy with [177Lu-DOTA]-TOC versus [90Y-DOTA]-TOC in neuroendocrine tumours.* Eur J Nucl Med Mol Imaging, 2014. **41**(2): p. 214-22.
24. Harald Schicha, O.S., Markus Dietlein, Wolfgang Eschner, Carsten Kobe, Klaus Kopka, Bernd Neumaier, Burkhard Riemann, MAtthias Schmidt, Lars Stegger, Mathias Weckesser, *Nuklearmedizin Basiswissen und klinische Anwendung*. Vol. 7. Auflage. 2013: Schattauer.
25. Warburg, O., *On the origin of cancer cells.* Science, 1956. **123**(3191): p. 309-14.
26. Mizutani, G., et al., *Expression of Somatostatin Receptor (SSTR) Subtypes (SSTR-1, 2A, 3, 4 and 5) in Neuroendocrine Tumors Using Real-time RT-PCR Method and Immunohistochemistry.* Acta Histochem Cytochem, 2012. **45**(3): p. 167-76.
27. Poeppel, T.D., et al., *68Ga-DOTATOC versus 68Ga-DOTATATE PET/CT in functional imaging of neuroendocrine tumors.* J Nucl Med, 2011. **52**(12): p. 1864-70.
28. *Number of positron emission tomography (PET) scan examinations in Germany from 2005 to 2017*. Available from: https://www.statista.com/statistics/963067/pet-scan-examinations-in-germany/.
29. Kinahan, P.E. and J.W. Fletcher, *Positron emission tomography-computed tomography standardized uptake values in clinical practice and assessing response to therapy.* Semin Ultrasound CT MR, 2010. **31**(6): p. 496-505.
30. Foster, B., et al., *A review on segmentation of positron emission tomography images.* Comput Biol Med, 2014. **50**: p. 76-96.
31. Abdulrezzak, U., et al., *Combined imaging with 68Ga-DOTA-TATE and 18F-FDG PET/CT on the basis of volumetric parameters in neuroendocrine tumors.* Nucl Med Commun, 2016. **37**(8): p. 874-81.
32. Erdi, Y.E., et al., *Segmentation of lung lesion volume by adaptive positron emission tomography image thresholding.* Cancer, 1997. **80**(12 Suppl): p. 2505-9.
33. Collarino, A., et al., *Experimental validation of absolute SPECT/CT quantification for response monitoring in breast cancer.* Med Phys, 2018. **45**(5): p. 2143-2153.
34. Aksu, A., et al., *Evaluation of 68Ga-PSMA PET/CT with volumetric parameters for staging of prostate cancer patients.* Nucl Med Commun, 2021. **42**(5): p. 503-509.
35. Draulans, C., et al., *Optimal (68)Ga-PSMA and (18)F-PSMA PET window levelling for gross tumour volume delineation in primary prostate cancer.* Eur J Nucl Med Mol Imaging, 2021. **48**(4): p. 1211-1218.
36. Reddy, R., et al., *Functional tumor volume measurement in Ga-DOTATATE PET-CT: Which method is correct?* 2020. **61**(supplement 1): p. 1306-1306.
37. Reddy, R.P., et al., *The quest for an accurate functional tumor volume with (68)Ga-DOTATATE PET/CT.* J Nucl Med, 2021.
38. Capobianco, N., et al., *Deep-Learning (18)F-FDG Uptake Classification Enables Total Metabolic Tumor Volume Estimation in Diffuse Large B-Cell Lymphoma.* J Nucl Med, 2021. **62**(1): p. 30-36.
39. O, J.H., M.A. Lodge, and R.L. Wahl, *Practical PERCIST: A Simplified Guide to PET Response Criteria in Solid Tumors 1.0.* Radiology, 2016. **280**(2): p. 576-84.
40. Gafita, A., et al., *qPSMA: Semiautomatic Software for Whole-Body Tumor Burden Assessment in Prostate Cancer Using (68)Ga-PSMA11 PET/CT.* J Nucl Med, 2019. **60**(9): p. 1277-1283.
41. Yasaka, K., et al., *Deep learning with convolutional neural network in radiology.* Jpn J Radiol, 2018. **36**(4): p. 257-272.

42. Pinochet, P., et al., *Evaluation of an Automatic Classification Algorithm Using Convolutional Neural Networks in Oncological Positron Emission Tomography.* Front Med (Lausanne), 2021. **8**: p. 628179.
43. Mercieca, S., et al., *Comparison of SUVmax and SUVpeak based segmentation to determine primary lung tumour volume on FDG PET-CT correlated with pathology data.* Radiother Oncol, 2018. **129**(2): p. 227-233.
44. Wahl, R.L., et al., *From RECIST to PERCIST: Evolving Considerations for PET response criteria in solid tumors.* J Nucl Med, 2009. **50 Suppl 1**: p. 122S-50S.
45. Yanarates, A. and E. Budak, *Prognostic role of PET/CT in endometrial cancer.* Ginekol Pol, 2019. **90**(9): p. 491-495.
46. Therneau, T.M. *A Package for Survival Analysis in R*. 2022; Available from: https://CRAN.R-project.org/package=survival.
47. Terry M. Therneau, P.M.G., *Modeling Survival Data: Extending the Cox Model*. 2000, New York: Springer.
48. Ambrosini, V., et al., *Prognostic Value of 68Ga-DOTANOC PET/CT SUVmax in Patients with Neuroendocrine Tumors of the Pancreas.* J Nucl Med, 2015. **56**(12): p. 1843-8.
49. Kaemmerer, D., et al., *Inverse expression of somatostatin and CXCR4 chemokine receptors in gastroenteropancreatic neuroendocrine neoplasms of different malignancy.* Oncotarget, 2015. **6**(29): p. 27566-79.
50. Bahri, H., et al., *High prognostic value of 18F-FDG PET for metastatic gastroenteropancreatic neuroendocrine tumors: a long-term evaluation.* J Nucl Med, 2014. **55**(11): p. 1786-90.
51. Refardt, J., et al., *Inferior outcome of neuroendocrine tumor patients negative on somatostatin receptor imaging.* Endocr Relat Cancer, 2020. **27**(11): p. 615-624.
52. Sharma, P., et al., *Comparison of the prognostic values of 68Ga-DOTANOC PET/CT and 18F-FDG PET/CT in patients with well-differentiated neuroendocrine tumor.* Eur J Nucl Med Mol Imaging, 2014. **41**(12): p. 2194-202.
53. Pace, L., et al., *Comparison of whole-body PET/CT and PET/MRI in breast cancer patients: lesion detection and quantitation of 18F-deoxyglucose uptake in lesions and in normal organ tissues.* Eur J Radiol, 2014. **83**(2): p. 289-96.
54. Watzka, F.M., et al., *Surgical therapy of neuroendocrine neoplasm with hepatic metastasis: patient selection and prognosis.* Langenbecks Arch Surg, 2015. **400**(3): p. 349-58.
55. Watzka, F.M., et al., *Surgical Treatment of NEN of Small Bowel: A Retrospective Analysis.* World J Surg, 2016. **40**(3): p. 749-58.
56. Begum, N., et al., *Long-term outcome of surgical resection in patients with gastroenteropancreatic neuroendocrine neoplasia: results from a German nation-wide multi-centric registry.* Langenbecks Arch Surg, 2020. **405**(2): p. 145-154.
57. Low, S.K., et al., *Competing Mortality in Patients With Neuroendocrine Tumors.* Am J Clin Oncol, 2019. **42**(8): p. 668-674.
58. Man, D., et al., *Prognosis of patients with neuroendocrine tumor: a SEER database analysis.* Cancer Manag Res, 2018. **10**: p. 5629-5638.
59. Zandee, W.T., et al., *Effect of hormone secretory syndromes on neuroendocrine tumor prognosis.* Endocr Relat Cancer, 2017. **24**(7): p. R261-R274.
60. uploader, C.R.U., *Diagram showing the parts of the body neuroendocrine tumours most commonly develop in CRUK 463.svg.* 13 January 2016.
61. Janet Pollard MD, M.S.O.D.M., PhD, Thomas O'Dorisio MD & Yusuf Menda MD, *Diagnostic and Therapeutic Nuclear Medicine for Neuroendocrine Tumors*. Contemporary Endocrinology. 2017.